Insulin Induces Microtubule Stabilization and Regulates the Microtubule Plus-End Tracking Protein Network in Adipocytes

Sara S. Parker[‡†], James Krantz[§†], Eun-A Kwak[Ψ], Natalie K. Barker[§], Chris G. Deer[¥], Nam Y. Lee[Ψ,ξ], Ghassan Mouneimne[‡] and Paul R. Langlais[§*]

[§] Department of Medicine, Division of Endocrinology, University of Arizona College of Medicine, Tucson, Arizona 85721

[‡] Department of Cellular & Molecular Medicine, University of Arizona College of Medicine, Tucson, Arizona 85721

[Ψ] Department of Pharmacology, University of Arizona College of Medicine, Tucson, Arizona 85721

[ξ] Department of Chemistry & Biochemistry, University of Arizona College of Medicine, Tucson, Arizona 85721

[¥] University of Arizona Research Computing, University of Arizona, Tucson, Arizona 85721

[†]Co-first authors

[*]To whom correspondence should be addressed: Department of Medicine, Division of Endocrinology, University of Arizona College of Medicine, 1501 N. Campbell Ave, Tucson, Arizona 85721

Phone: 520-626-1342

E-mail: langlais@deptofmed.arizona.edu

Running title: The Effect of Insulin on Microtubule-Associated Proteins

The abbreviations used are:

+TIP Plus-end tracking microtubule-associated protein

AcK40 α-tubulin lysine 40 acetylation

AGAP3 Arf-GAP with GTPase, ANK repeat, and PH domain-containing protein 3

ANK ankyrin

AP-MS affinity purification coupled with mass spectrometry

BAS basal

CAP-Gly cytoskeleton-associated protein Gly-rich

CKAP5 cytoskeleton-associated protein 5

CLASP1 CLIP-associating protein 1

CLASP2 CLIP-associating protein 2

CLIP1/CLIP-170 CAP-Gly domain-containing linker protein 1

CLIP2/CLIP-115 CAP-Gly domain-containing linker protein 2

co-IP(s) co-immunoprecipitation(s)

CTCF corrected total cell fluorescence

CTRL control

EB1 end binding protein 1

EB3 end binding protein 3

EBH EB homology

EEY/F EEY/F motif

FA formic acid

GAP GTPase-activating protein

GAR Gas2-related

GAS2 growth-arrest-specific 2

GAS2L1/G2L1 GAS2 like protein 1

GFP green fluorescent protein

GLD GTP-binding protein-like domain

GLUT4 solute carrier family 2, facilitated glucose transporter member 4

GSK3 glycogen synthase kinase 3

HA hemagglutinin

ID identification

INS insulin

IP(s) immunoprecipitation(s)

KA1 kinase associated domain 1

MAP microtubule associated protein

MARK2 microtubule affinity-regulating kinase 2

MK protein ladder marker

MS/MS tandem mass spectrometry

NIgG non-immune serum

NOCO nocodazole

PH pleckstrin homology

P-Score probability score

ROI region of interest

SAINT significance analysis of interactome

SB SB216763

SC spectrum count

SCP spectrum count profile

SD standard deviation

SEM standard error of the mean

TOG tumor overexpressed gene

TIRFM total internal reflection fluorescence microscopy

UBA ubiquitin-associated

WCL whole cell lysate

SUMMARY

Insulin-stimulated glucose uptake is known to involve microtubules, although the function of microtubules and the microtubule-regulating proteins involved in insulin action are poorly understood. CLASP2, a plus-end tracking microtubule-associated protein (+TIP) that controls microtubule dynamics, was recently implicated as the first +TIP associated with insulin-regulated glucose uptake. Here, using protein-specific targeted quantitative phosphoproteomics within 3T3-L1 adipocytes, we discovered that insulin regulates phosphorylation of the CLASP2 network members G2L1, MARK2, CLIP2, AGAP3 and CKAP5 as well as EB1, revealing the existence of a previously unknown microtubule-associated protein system that responds to insulin. To further investigate, G2L1 interactome studies within 3T3-L1 adipocytes revealed that G2L1 co-immunoprecipitates CLASP2 and CLIP2 as well as the master integrators of +TIP assembly, the end binding (EB) proteins. Live-cell total internal reflection fluorescence microscopy in adipocytes revealed G2L1 and CLASP2 colocalize on microtubule plus-ends. We found that while insulin increases the number of CLASP2-containing plus-ends, insulin treatment simultaneously decreases CLASP2-containing plus-end velocity. In addition, we discovered that insulin stimulates re-distribution of CLASP2 and G2L1 from exclusive plus-end tracking to “trailing” behind the growing tip of the microtubule. Insulin treatment increases α-tubulin Lysine 40 acetylation, a mechanism that was observed to be regulated by a counterbalance between GSK3 and mTOR, and also led to microtubule stabilization**.** Our studies introduce insulin-stimulated microtubule stabilization and plus-end trailing of +TIPs as new modes of insulin action and reveal the likelihood that a network of microtubule-associated proteins synergize to coordinate insulin-regulated microtubule dynamics.

INTRODUCTION

Since the initial discovery of insulin-stimulated cytoskeletal remodelling over 25 years ago (1), the role of both actin and microtubule reorganization in insulin action and the proteins that regulate these processes have been the subject of investigation. Upon insulin stimulation, cell models of insulin target tissues including 3T3- L1 adipocytes as well as L6 and C2C12 myotubes (2-6) exhibit profound actin reorganization at the plasma membrane as a result of actin branching. Rac1 is a master regulator of actin dynamics and inhibiting either Rac1 or Rac1-effector proteins severely diminishes trafficking of the insulin responsive glucose transporter (Solute carrier family 2, facilitated glucose transporter member 4 or "GLUT4") and subsequent insulin-stimulated glucose uptake (7). Therefore, insulin not only relies on signal transduction through protein-protein communication, but also requires a specific cytoskeletal environment to properly enhance acute glucose uptake. Studies characterizing the proteins involved in insulin-controlled actin regulation have been more prevalent than those focused on proteins involved in regulating microtubule dynamics upon insulin stimulation. As a result, much more progress has been made on elucidating the actin system under insulin control versus that of microtubules.

Microtubules possess the unique characteristic of "dynamic instability", their growth and shrinkage serve as modes of functional regulation across a multitude of molecular platforms. Microtubule assembly and disassembly rates as well as duration of stability are controlled in part by "microtubule-associated proteins" (MAPs), a large family of proteins with several notable sub-groups (reviewed in (8)). While many of the MAPs localize at the base of the microtubule (the minus-end) or along the length of the microtubules (the lattice), the plus-end tracking proteins (+TIPs) are found at the growing tip of the microtubule (the plus-end). The +TIPs are a functionally diverse group of almost 20 proteins, and as such, their regulation and cooperativity have been explored at length (reviewed in (9)), although not in the context of insulin action. One exception is CLIP-associating protein 2 (CLASP2) (10), a +TIP that was found to be enriched in an unbiased proteomics screen for proteins that undergo insulin-stimulated phosphorylation (11). Just like the

rest of the +TIPs, CLASP2 tracks the plus-end of microtubules, associates with an assortment of other +TIPs, and is involved in a variety of microtubule-regulated cellular events (12). Notably, CLASP2 has been linked to the “search and capture” behaviour of microtubules (13), wherein microtubule tips are observed to seek out specific landing zones through CLASP2 binding of proteins localized at particular subcellular regions (14-18). For example, CLASP2 binding to microtubule capture sites on the cell cortex creates a delivery route for acetylcholine receptors to neuromuscular junctions (19) as well as exocytotic vesicles traveling to focal adhesions (20). These observations revealed that under certain cellular contexts, microtubules adopt specific patterns of reorganization which possess both temporal and spatial characteristics that synchronize with +TIP function.

Microtubules and actin routinely cooperate through proteins including the formins (21), the spectraplakins (22), and members of the growth-arrest-specific 2 (GAS2) family (23). One of the GAS2 family members, G2L1, was recently discovered in the CLASP2 interactome in 3T3-L1 adipocytes (24). G2L1 interacts with both actin and microtubules to coordinate actin and microtubule alignment (23, 25, 26), an event that is of potential interest within insulin action since the insulin-responsive GLUT4 storage vesicle has been proposed to switch tracks at an interface between microtubules and actin at the plasma membrane (27).

Early immunofluorescence studies coupled with biochemical techniques first discovered that insulin increases tubulin polymerization in 3T3-L1 adipocytes (28). A decade later, using live-cell total internal reflection fluorescence (TIRF) microscopy, it was demonstrated that insulin increases microtubule density and curvature in the 200nm immediately proximal to the plasma membrane in 3T3-L1 adipocytes (29). The purpose of these dynamic microtubule events has never been established and the mechanisms underlying microtubule regulation in insulin action are still unknown. This report presents new findings that significantly expand the number of +TIPs affected by insulin, evidence for the existence of an undiscovered microtubule-associated protein system under insulin control. We found that insulin stimulation promotes a re-distribution of

CLASP2 and G2L1 from exclusive microtubule plus-end localization to “trailing” behind the growing tip of the microtubule along the microtubule lattice. We discovered that insulin acutely stimulates acetylation of α-tubulin at Lysine 40 and promotes microtubule stabilization, a phenomenon never before linked to acute insulin action. Our studies introduce a new insulin-responsive protein system as well as novel insulin-regulated microtubule and microtubule-associated protein dynamics, findings that significantly expand our understanding of the relationship between insulin and the microtubule network.

EXPERIMENTAL PROCEDURES

Cell Culture, Immunoprecipitation, and Western Blot Analysis. Mouse 3T3-L1 fibroblasts were differentiated into adipocytes exactly as previously described (24). For cell treatment experiments, cells were starved for four hours in serum free media containing 0.3% BSA and then either left untreated or stimulated with 100 nM insulin for 15 min (unless otherwise indicated) at 37 °C. Cells were lysed with 500 μL of lysis buffer containing 40 mM HEPES (pH 7.6), 120 mM NaCl, 0.3% CHAPS, 10 mM NaF, 10 mM β-glycerol phosphate, 1 mM EDTA (pH 8.0), 2 mM sodium orthovanadate, 17 μg/ml aprotinin, 10 μg/ml leupeptin, and 1 mM PMSF. Cell lysates were rotated at 4 °C for 20 min followed by centrifugation (14,000 RPM, 4 °C, 20 min), and the clarified supernatants were used for immunoprecipitation (IP). IPs and preparation for SDS-PAGE were performed exactly as previously described (24). The eluates were separated by 10% SDS-PAGE and the gels were either stained with Bio-Safe Coomassie G-250 Stain (Bio-Rad, Hercules, CA) or transferred to a nitrocellulose membrane for subsequent western blotting. Western blots were performed exactly as previously described (24). Primary antibodies used: anti-G2L1 (cat. # H00010634-B01P, Novus Biologicals, Littleton, CO), anti-mCherry (cat. # NBP2-43720, Novus Biologicals), anti-myc (cat. # 2276, Cell Signaling Technologies, Danvers, MA), anti-EB1 (cat # E3406, Sigma-Aldrich, St. Louis, MO), anti-α-tubulin (cat. # T9026, Sigma-Aldrich), anti-acetylated Lysine 40 of α-tubulin (“AcK40”) (cat. # 5335, Cell Signaling Technologies), anti-

MARK2 (cat. # NBP1-71890, Novus Biologicals), anti-CLIP2 (cat. # SAB1412760, Sigma Aldrich), anti-AGAP3 (cat. # SAB2700915, Sigma Aldrich), and anti-CKAP5 (cat. # 620401, Biolegend).

In-gel Digestion. Proteins were separated by SDS-PAGE and stained with Bio-Safe Coomassie G-250 Stain. For the interactome experiments, each lane of the SDS-PAGE gel was cut into seven slices. For the specific protein targeted phosphoproteomics experiments, the single band corresponding to the location of the individual protein on the SDS-PAGE gel was excised. The gel slices were subjected to trypsin digestion and the resulting peptides were purified by C18-based desalting exactly as previously described (24). The dried peptides were resuspended in 6 μl of 0.1% FA (v/v) followed by sonication for 2 min. 2.5 μl of the final sample was then analyzed by mass spectrometry.

Mass Spectrometry and Spectrum Count Data Processing. HPLC-ESI-MS/MS was performed in positive ion mode on a Thermo Scientific Orbitrap Fusion Lumos tribrid mass spectrometer fitted with an EASY-Spray Source (Thermo Scientific, San Jose, CA). NanoLC was performed without a trap column using a Thermo Scientific UltiMate 3000 RSLCnano System with an EASY Spray C18 LC column (Thermo Scientific, 50cm x 75 μm inner diameter, packed with PepMap RSLC C18 material, 2 μm, cat. # ES803); loading phase for 15 min at 0.300μL/min; mobile phase, linear gradient of 1–34% Buffer B in 119 min at 0.220 μL/min, followed by a step to 95% Buffer B over 4 min at 0.220 μL/min, hold 5 min at 0.250 μL/min, and then a step to 1% Buffer B over 5 min at 0.250 μL/min and a final hold for 10 min (total run 159 min); Buffer A = 0.1% FA/H_2O; Buffer B = 0.1% FA in 80% ACN. All solvents were liquid chromatography mass spectrometry grade. Spectra were acquired using XCalibur, version 2.3 (Thermo Scientific). A “top speed” data-dependent MS/MS analysis was performed. Dynamic exclusion was enabled with a repeat count of 1, a repeat duration of 30 sec, and an exclusion duration of 60 sec. Tandem mass spectra were extracted from Xcalibur ‘RAW’ files and charge states were assigned using the ProteoWizard 3.0.1 msConvert script using the default parameters (30). The fragment mass

spectra were then searched against the mouse SwissProt_2016_10 database (23,550 entries) using Mascot (Matrix Science, London, UK; version 2.4) using the default probability cut-off score. The search variables that were used were: 10 ppm mass tolerance for precursor ion masses and 0.5 Da for product ion masses; digestion with trypsin; a maximum of two missed tryptic cleavages; variable modifications of oxidation of methionine and phosphorylation of serine, threonine, and tyrosine. Cross-correlation of Mascot search results with X! Tandem was accomplished with Scaffold (version Scaffold_4.8.7; Proteome Software, Portland, OR, USA). Probability assessment of peptide assignments and protein identifications were made through the use of Scaffold. Only peptides with ≥ 95% probability were considered. Reported peptide FDR rates from Scaffold ranged from 0.1-0.2%. The mass spectrometry proteomics data have been deposited to the ProteomeXchange Consortium via the PRIDE partner repository (31) with the dataset identifier PXD011431 and 10.6019/PXD011431. For the Spectrum Count Profiles, the Uniprot IDs are listed.

Label-free Quantitative Proteomics. Progenesis QI for proteomics software (version 2.4, Nonlinear Dynamics Ltd., Newcastle upon Tyne, UK) was used to perform ion-intensity based label-free quantification. In brief, in an automated format, .raw files were imported and converted into two-dimensional maps (y-axis = time, x-axis =m/z) followed by selection of a reference run for alignment purposes. An aggregate data set containing all peak information from all samples was created from the aligned runs, which was then further narrowed down by selecting only +2, +3, and +4 charged ions for further analysis. The samples were then grouped in basal versus insulin. A peak list of fragment ion spectra from only the top eight most intense precursors of a feature was exported in Mascot generic file (.mgf) format and searched against the mouse SwissProt_2016_10 (23,550 entries) database using Mascot (Matrix Science, London, UK; version 2.4). The search variables that were used were: 10 ppm mass tolerance for precursor ion masses and 0.5 Da for product ion masses; digestion with trypsin; a maximum of two missed tryptic cleavages; variable modifications of oxidation of methionine and phosphorylation of serine,

threonine, and tyrosine; 13C=1. The resulting Mascot .xml file was then imported into Progenesis, allowing for peptide/protein assignment, while peptides with a Mascot Ion Score of <25 were not considered for further analysis. Precursor ion-abundance values for specific phosphopeptide ions were normalized to a selected series of standard peptide ions for the same target protein. The selected series of standard peptide ions had to conform to a set of rules previously established (32-34), i.e. (1) detected by HPLC-ESI-MS with high intensity among the peptides for the target protein; (2) no missed cleavage observed; (3) no methionine in the sequence to avoid variability due to methionine oxidization and no N-terminal Gln residues; (4) cannot be a non-phosphorylated version of a peptide that was detected as being phosphorylated. Each phosphopeptide ion's normalized abundance value was normalized by the mean value of the respective basal sample and then expressed as a fold change over basal ±SEM. When multiple peptide ions were present for a particular phosphopeptide ion, a representative peptide ion was chosen to reflect the effect of insulin. For the proof of principle dose curve test, no normalization was performed.

Generation of Viruses and transduction of 3T3-L1 Adipocytes. Negative control null GFP adenovirus as well as N-terminal GFP plus C-terminal HA-tagged mouse CLASP2 adenovirus were described before (24). Negative control null mCherry adenovirus as well as N-terminal mCherry plus C-terminal myc-tagged mouse G2L1 adenovirus using G2L1 cDNA, cat. # MC204613 from Origene (Rockville, MD) were created by VECTOR BIOLABS (Malvern, PA). Viral infections were performed on 150 mm plates of 3T3-L1 adipocytes as previously described (24). Lentiviral transfer plasmid pCIG3 (Addgene #78264, a gift from Felicia Goodrum) was modified to express a puromycin resistance gene in place of GFP. mRuby2-Tubulin-6 (human Tubulin alpha 1b; Addgene #55914, a gift from Michael Davidson) was subcloned into this backbone by addition of the restriction sites KpnI and BamHI by PCR, to generate pLenti-mRuby2-Tubulin. To generate pLenti-iRFP670-Tubulin, tubulin was first subcloned out of the mRuby2-Tubulin-6 vector and into piRFP670-N1 (Addgene #45457, a gift from Vladislav

Verkhusha). iRFP670-Tubulin was then subcloned out of the piRFP670-Tubulin vector and into the pLenti backbone to generate pLenti-iRFP670-Tubulin. Second generation lentiviral particles were generated by PEI transfection of 293T cells as previously described (35) with transfer plasmid, pMD2.G, and psPAX2 (Addgene #12259, #12260, gifts from Didier Trono). At 48 and 72 hours post-transfection, 293T media containing lentiviral particles was collected and combined followed by centrifugation at 500 x g for 15 minutes. The supernatant was filtered and either immediately used or concentrated (Lenti Concentrator, cat. # TR30025, Origene), depending on the virus. The virus was added directly to adipocyte cultures with polybrene. The following day, cells were split onto Poly-D-Lysine (cat. # A-003-E, Sigma Aldrich) treated glass bottom dishes (cat. # P35GCol-1.5-14-C, MatTek Corporation), and the cells were imaged 24 hours later.

Immunofluorescence and Live-Cell Imaging. For live-cell imaging experiments, cells were cultured on No. 1.5 coverslip bottom dishes (Mattek, Ashland, MA). Adipocytes were starved for one hour in serum free media containing 0.3% BSA and then either left untreated or stimulated with 100 nM insulin for the indicated duration at 37 °C. For immunofluorescence studies, 3T3-L1 adipocytes were split onto coverslips (cat. # 1254580, Fisher Scientific). The following day, the cells were starved for 4 hours in serum free media containing 0.3% BSA followed by the indicated cell treatments. Cells were fixed with 100%, -20 °C methanol for 20 minutes followed by permeabilization with 1% Tween-20 and 2% PFA. The background signal was quenched with 0.1 M glycine followed by incubation in 1% BSA. Coverslips were incubated with anti-α-Tubulin and anti-AcK40 Tubulin, followed by incubation with 568 anti-mouse (cat. # A10037, Life Technologies) and 488 anti-rabbit (cat. # A11034, Life Technologies) secondary antibodies, and then mounted onto slides with ProLong Diamond (cat. # p36965, Fisher Scientific).

Microscopy and Image Analysis. Total Internal Reflection Fluorescence Microcopy was performed on a Nikon Eclipse Ti (Nikon Instruments Inc., Melville, NY) inverted microscope equipped with multiple laser lines with AOTF control, Nikon Perfect Focus System, and an environmental chamber supplying 5% CO2 and 37°C temperature control. Samples were imaged

with a 100X Apo TIRF 1.49 NA oil-immersion objective. TIRF excitation angle was determined by adjusting for maximum extinction. Image acquisition was performed using a Hamamatsu ORCA-Flash 4.0 V2 cMOS camera (Hamamatsu Photonics). Live images were acquired on a 2 second interval for the indicated total duration. Images were deconvolved in NIS Elements using five iterations of Richardson-Lucy deconvolution algorithm. Overall microtubule structure and acetylation were imaged using a Zeiss Axio Observer 7- ApoTome.2 inverted microscope with 63X oil-immersion objective and Axiocam 503 mono camera. Microscopy figures and videos were prepared using ImageJ/FIJI (36) and Adobe Photoshop. For the quantification of the time courses on the effect of insulin on CLASP2 and G2L1 trailing, the live cell images were analyzed using Imaris 9.2.1 with FIJI extension. Specifically, +TIP microtubule decoration lengths were measured at different time points at fixed intervals with respect to the length of the time course using a frame within the first minute. The manual filament tools of Imaris were used for measurement of +TIP trail lengths, which were identified by scrubbing the time slider. Measurement was done visually, starting at the moving end of the trail or trail break with the AutoPath feature of Imaris. Once all visible trails were measured on frame, a new filament object was created and time was scrubbed to the next frame along the fixed interval specified earlier. After image analysis was completed, all filament objects were compared to the serum-starved length of the first frame using Imaris Vantage. +TIP length data was graphed using RStudio. For quantification of +TIP velocity, CLASP2 position was tracked during a 30-second imaging interval using the Manual Tracking FIJI plug-in. The density of +TIPs was quantified by manually counting motile CLASP2 signal on microtubules, and normalizing to cell area. For quantification of tubulin stabilization after nocodazole treatment with or without insulin treatment, the length of the microtubule network was measured using Simple Neurite Tracer FIJI plug-in (37), and normalized to cell area. Quantification for microtubule acetylation was determined using ImageJ corrected total cell fluorescence (CTCF) which calculates the normalized fluorescence based on the formula (Integrated density – (Area of selected cell x Mean background fluorescence) (38).

Experimental Design and Statistical Rationale. Previous interactome experiments using the mean and standard deviations for the spectrum counts of proteins identified by SAINT analysis as significantly enriched over the negative control showed a sample size of four biological replicates per group provided more than sufficient power to detect differences between groups (24). Based on the high degree of reproducibility, we used a sample size of two biological replicates for the interactome experiments and followed those experiments with confirmatory reciprocal interactomes as well as IP and western blots to further validate potential protein partners. The varying statistical analyzes for the remainder of the other types of experiments are listed in the Figure Legends and were justifiable based upon the data and basic experiment performed. For spectral counting measurements, modified peptides, semi-tryptic peptides, and shared peptides were included. Statistical analysis of +TIP density, +TIP velocity, and tubulin stabilization experiments was performed by confirming the distribution of the data by Shapiro-Wilk normality test, and performing a paired or unpaired t-test as indicated. Statistical analysis of CTCF and +TIP microtubule decoration lengths was performed by a paired or unpaired t-test as indicated

RESULTS

Insulin Regulates the Phosphorylation of G2L1, MARK2, CLIP2, EB1, AGAP3, and CKAP5 - We recently reported characterization of a CLASP2 protein network in 3T3-L1 adipocytes (24), and since we previously detected CLASP2 in an unbiased proteomics screen for proteins that undergo insulin-stimulated phosphorylation (11), we hypothesized that the members of the CLASP2 network in 3T3-L1 adipocytes (24) also undergo insulin-regulated phosphorylation. We adapted our previously reported technique (32-34, 39) of label-free quantification of phosphorylation, where extracted ion abundances from parent ion phosphopeptides are normalized to parent ion peptides of the same protein, except we now take advantage of automated processing of the data using Progenesis (Figure 1A). We validated the quantitative

approach via Progenesis using immunoprecipitated CLASP2 digests (Supplemental Figure 1). Upon stimulating 3T3-L1 adipocytes with insulin, we discovered that the CLASP2 protein network members G2L1, CLIP2, AGAP3, MARK2 and CKAP5 all undergo insulin-regulated phosphorylation, as well as EB1, a fundamental +TIP with ties to CLASP2, G2L1, CLIP2 and CKAP5 (40) (Figure 1B-C, Supplemental Figure 2, and Supplemental Tables 1-6). These findings highlight a completely new series of proteins that are responsive to insulin and reveal the existence of a systematic microtubule-regulating protein response to insulin.

The G2L1 Interactomes - We previously characterized the CLASP2 protein network in 3T3-L1 adipocytes and discovered G2L1 was enriched in three alternative, cross-reference CLASP2 interactomes (24). To follow-up on a possible relationship between CLASP2 and G2L1 in 3T3-L1 adipocytes, we performed multiple G2L1 affinity purification coupled with mass spectrometry (AP-MS) experiments using our previously described label-free quantitative proteomics approach (24) (Figure 2A). We performed basal versus insulin treatment interactome analysis of endogenous G2L1 IPs as well as overexpressed G2L1 immunoprecipitated with two alternative antibodies, one to a myc-epitope tag and the other to a mCherry fluorescent protein tag (western blots of all G2L1 protein IPs are shown in Figure 2B). The resulting spectrum count data for the G2L1 IPs was then scored for enrichment over the various appropriate negative control IPs using the established bioinformatic tool Significance Analysis of Interactome (SAINT) as previously described (24, 41-43). On the SAINT Probability Score ("P-Score") scale from 0 to 1, ≥0.85 was used to signify a protein as "SAINT qualified". Protein SAINT scores, spectrum counts, distinct peptides, and percent protein coverage for the interactomes are included in the Supplemental Tables 7-15. We used our Spectrum Count Profile ("SCP") to hierarchically summarize the raw spectral count data of all the SAINT-qualified proteins (Figure 2C) followed by Cytoscape-based (44) integration to simultaneously visualize all three G2L1 SAINT-qualified interactomes (Figure 2D). All three G2L1 interactomes (Uniprot ID for G2L1 is GA2L1) had SAINT-

qualified enrichment of CLASP2 and CLIP2, discoveries which serve to reciprocally confirm our previous report that both CLASP2 and CLIP2 can co-IP G2L1 (24). G2L1 was identified during a proteome-wide screen for EB-binding proteins (26). In our overexpressed G2L1 interactomes, EB1 (Uniprot ID: MARE1) and to a lesser extent EB3 (Uniprot ID: MARE3) were both strongly enriched, with spectrum count numbers similar to those detected for CLASP2. CLASP2 at a predicted mass of ~141kDa has the potential for a larger number of spectrum counts compared to EB1 at ~30kDa, so the fact that EB1 and CLASP2 had comparable spectrum counts suggests a larger amount of EB1 associates with G2L1 versus CLASP2 (as well as CLIP2). Antibodies targeted to endogenous protein can disrupt protein-protein interactions and possess non-specific cross-reactivity (45, 46), which may explain why EB1 was undetected in the endogenous G2L1 interactome. In order to further validate the association between EB1 and G2L1, we performed an endogenous EB1 interactome and confirmed the reciprocal co-IP of G2L1 with EB1 (Supplemental Figure 3). The overexpressed G2L1 interactomes possessed levels of CLASP1 similar to those detected for CLASP2, EB1, and CLIP2 and contained a lower amount of EB3 as compared to EB1. There were other similarities between the two overexpressed G2L1 interactomes, including the presence of five members (APC1, ANC2/APC2, APC4, APC5, and CDC23) of the anaphase promoting complex/cyclosome (APC), an E3 ubiquitin ligase that facilitates ubiquitination and degradation of target proteins (47). There were also differences in the two overexpressed G2L1 interactomes that may have resulted from steric hindrance caused by antibody binding.

To follow up on the G2L1 interactome findings, we performed traditional co-IP and western blot experiments and focused on confirmatory tests for the association of G2L1 together with CLASP2, CLIP2, and EB1. We reproduced the interactome data and reciprocally confirmed the interactions between G2L1 and CLASP2, CLIP2, and EB1 (Supplemental Figure 4). We also found no significant effect of insulin on the reciprocal interactions, findings that are similar to those

observed in the interactome studies. Collectively, we have established a new relationship between G2L1 and CLASP2, CLIP2, and EB1 in 3T3-L1 adipocytes.

Colocalization of CLASP2 and G2L1 - CLASP2 and G2L1 are reciprocally enriched in the interactome studies we have performed, evidence that supports potential biological cooperation between these two +TIPs. We therefore tested for colocalization of CLASP2 and G2L1 in basal state 3T3-L1 adipocytes proximal to the cell membrane using live-cell total internal reflection fluorescence microscopy (TIRFM), a powerful tool for visualizing +TIP localization and microtubule dynamics. Overexpression of either GFP-CLASP2-HA (Figure 3A) or mCherry-G2L1-myc (Figure 3B) in 3T3-L1 adipocytes revealed that each protein localizes to the growing plus-end of microtubules within comet-like structures, which can be observed tracking across the cell and leading a newly formed microtubule, per classic +TIP behavior. When co-expressed, CLASP2 and G2L1 are coincident on dynamic comet-like structures (Video 1). Examination of fixed samples of adipocytes co-expressing GFP-CLASP2 and mCherry-G2L1 revealed that comparatively, G2L1 occupies a smaller and more proximal area of the +TIP than CLASP2, which led a longer comet-like structure on microtubules (Figure 3C). These additional findings validate the interactome data and solidify a potential cooperative relationship between CLASP2 and G2L1.

The Effect of Insulin on CLASP2 and G2L1 +TIP Dynamics - Upon successfully establishing colocalization of CLASP2 and G2L1 with TIRFM in 3T3-L1 adipocytes, as well as discovering that both CLASP2 (11) and G2L1 undergo insulin-regulated phosphorylation, we profiled the effect of insulin on CLASP2 and G2L1 cellular localization proximal to the inner surface of the plasma membrane in a live-cell setting. Microtubule polymerization and density have both been shown to increase after insulin treatment in 3T3-L1 adipocytes (28, 29). Comparative quantification revealed that insulin increases the number of CLASP2-containing +TIPs per unit area (Figure 4A-B), data that aligns with the previous findings that insulin increases microtubule density. Conversely, we discovered that insulin treatment reduces the average

velocity of CLASP2-containing +TIPs (Figure 4C-D), suggesting that insulin slows the polymerization rate of individual microtubules with CLASP2-containing +TIPs. Taken together our data aligns with pre-existing findings that insulin increases the population of microtubules. While this implicates insulin increases gross microtubule polymerization, we propose that while insulin may create more microtubules, microtubules that possess CLASP2-containing +TIPs polymerize slower in the presence of insulin.

Prior to insulin treatment, CLASP2 moves in short, rapid bursts with a comet-like appearance per classic +TIP presentation (Video 2). After insulin stimulation, we discovered that CLASP2 shifts from being exclusively enriched at the plus-end microtubule tip to “trailing”, in which CLASP2 decorates the trailing length of the microtubule proximal to the growing plus-end (Video 2, Figure 4E-G, Supplemental Figure 5). Since we observed G2L1 co-localizes with CLASP2 in adipocytes, we hypothesized that G2L1 behavior might also respond to insulin stimulation. In the basal state G2L1 displays classic +TIP activity (Video 3) whereas insulin stimulates G2L1 trailing on microtubules (Video 3, Figure 5A-C, Supplemental Figure 5). Insulin is known to stimulate membrane ruffling in adipocytes (4). Since G2L1 is known to localize to actin in addition to microtubules, it is of particular interest that upon insulin stimulation, G2L1 strongly enriches to lamellipodial protrusions (Video 3). Upon testing the effect of insulin on adipocytes co-expressing both GFP-CLASP2 and mCherry-G2L1, the insulin-stimulated trailing phenotype was definitively captured (Video 4, Figure 6A-C). Quantification of the +TIP trail length captured the trailing phenotype induced by insulin within each of the representative adipocytes (Figure 4G, Figure 5C and Figure 6C). In order to rule out insulin-stimulated +TIP trailing resulting from a phototoxic effect associated with continual exposure to laser light during live cell imaging, we have reproduced the findings in cells visualized for only thirty seconds at a time at five-minute intervals pre- and post-insulin stimulation (data not shown). The insulin-induced +TIP trailing response observed was not universal across all cells, perhaps due to the reported heterogeneous

nature of adipocyte differentiation (48). We present here, for the first time, that insulin affects CLASP2 and G2L1 +TIP dynamics (modelled in Figure 6D), direct evidence that supports the hypothesis that the +TIP network represents a new signaling system associated with insulin action.

Insulin Stimulates α-Tubulin Acetylation at Lysine 40 and Microtubule Stabilization - Results from the live cell experiments revealed that insulin stimulates CLASP2 and G2L1 to shift from predominant localization at the microtubule plus-end to trailing along varied lengths of the microtubule lattice proximal to the growing plus-end. Dynamic short-lived microtubules are characterized by transient periods of growth and shrinkage (49), although a subset of the microtubule population are stabilized and persist for much longer times as a means for long-range transport. These long-lived microtubules can possess α-tubulin acetylation at lysine 40 ("AcK40"), a post-translational modification that protects microtubules from mechanical stress (50, 51). Since the microtubules with insulin-stimulated CLASP2 and G2L1 trails visually presented as "brace-like" across the microtubule lattice, we first tested the hypothesis that insulin stimulates a marker for stabilized microtubules, AcK40. Western blot analysis of whole cell lysates from serum-starved 3T3-L1 adipocytes either left untreated or subjected to an insulin time course confirmed that insulin stimulates α-tubulin acetylation at lysine 40 ("AcK40") (Figure 7A), results that were reproduced with AcK40 immunofluorescence imaging (Figure 7B-C). Since an insulin-stimulated increase in AcK40 is not direct evidence of microtubule stabilization, we tested whether insulin treatment results in increased resistance to the microtubule depolymerizing agent, nocodazole. Treatment of serum-starved adipocytes with nocodazole induced a loss of microtubules, while pre-treatment of cells with insulin reduced the severity of nocodazole-stimulated microtubule depolymerization (Figure 7D-E), therefore, we conclude insulin increases the stability of microtubules in 3T3-L1 adipocytes.

To test for specificity of the AcK40 western blot signal and also to search for the pathway(s) involved in regulating insulin-controlled AcK40, we discovered we could inhibit the insulin-stimulated increase of AcK40 by treating the adipocytes with the mTOR inhibitor rapamycin (32% average decrease, n=7, $p \leq 0.01$), implicating mTOR in insulin-stimulated microtubule stabilization (Figure 7F). The kinase GSK3 has been linked to suppressing AcK40 in the context of cell polarization (10). Since GSK3 is active in the basal state and deactivated by insulin, we hypothesized that GSK3 regulates basal levels of microtubule stabilization through suppression of AcK40. Treatment of 3T3-L1 adipocytes with the GSK3 inhibitor SB216763 reversed the decreased levels of AcK40 observed in the basal state, indicating that insulin suppresses GSK3 activity in part to encourage an increase in AcK40 (Figure 7G and H). These discoveries reveal a whole new property of insulin, namely increased microtubule stabilization as well as the stimulation of α-tubulin acetylation at lysine 40, a generally accepted marker for microtubule stabilization, a mechanism that is regulated at least in part by a counterbalance between GSK3 and rapamycin-sensitive mTOR-controlled signaling elements (modelled in Figure 7I).

DISCUSSION

We followed up on our recent CLASP2 interactome study by characterizing the G2L1 interactome within 3T3-L1 adipocytes. The +TIPs have been an encouraging fit for interactome studies, as known positive control interaction partners have been routinely detected and reciprocal interactomes have been largely confirmatory. We reproduced results from other cell lines (23, 26) that G2L1 co-IPs EB1 and discovered that G2L1 also co-IPs both CLASP2 and CLIP2 in 3T3-L1 adipocytes, data which reciprocally confirms our previous CLASP2 and CLIP2 interactome findings (24). We performed an EB1 interactome and confirmed the reciprocal presence of G2L1, although, we did not detect significant enrichment of CLASP2 in the EB1

interactome. Prior experiments on EB1 and CLASP2 have supported the concept that these two proteins may track along growing microtubule plus-ends individually from each other, as was observed in PtK1 epithelial cells (52). The lack of a detectable strong co-IP between EB1 and CLASP2 in adipocytes is consistent with our previous CLASP2 interactome work (24) although discordant from a study in COS-1 cells which proved an interaction can occur between EB1 and CLASP2 (17). There have been repeated published links between CLASP2 and the EB proteins, including a dependence of EB1 proper microtubule localization on CLASP2 within a multitude of cell types (53). All of these observed differences in the relationship between EB1 and CLASP2 could be explained by cell-line specificity, a transient nature of association as previously proposed (17), a difference in the expression levels of other +TIPs necessary for assembling specific protein complexes (9, 40, 49, 54-56), a lack of detectable interactions resulting from technical limitations, or issues with the immunoprecipitating antibodies (45, 46). Future studies will investigate whether the lack of a detectable association between CLASP2 and EB1 indicates that G2L1 and EB1 may operate independently of CLASP2 in adipocytes and whether the G2L1/EB1 relationship is affected by insulin in a spatio-temporal manner. The link between G2L1 and CLASP2 discovered during the interactome studies was solidified by the live-cell TIRFM-based discovery that G2L1 and CLASP2 co-localize at growing microtubule plus-ends. In addition to localizing to microtubule plus-ends, G2L1 also possesses binding capacity for filamentous actin (F-actin) (23, 57, 58). We have unpublished findings indicating that in addition to the insulin-regulated +TIP characteristics observed for G2L1 reported here, G2L1 also colocalizes with insulin-stimulated actin reorganization and membrane ruffling. In addition, we have now established that both CLASP2 (11) and G2L1 undergo insulin-stimulated phosphorylation. Since insulin-stimulated actin reorganization is paramount for proper insulin action (7), future studies will elucidate whether a functional association exists between insulin-stimulated actin dynamics and G2L1.

The effect of insulin on both CLASP2 and G2L1 on microtubules proximal to the interior surface of the cell ("the TIRFM zone") represent a new mode of +TIP regulation in the context of insulin action. Live-cell TIRFM captured CLASP2 and G2L1 shifting from predominant plus-end localization to insulin-stimulated immobilization along the length of the microtubule lattice, proximal to the growing plus-end (modelled in Figure 6D). CLASP2 has repeatedly been linked to the stabilization of microtubules through participating in microtubule rescue events and preventing microtubule depolymerization, across multiple organisms (17, 56, 59-72). These effects are imparted through the various domains in CLASP2, for example, the tumor overexpressed gene 2 (TOG2) domain was recently shown to maintain the integrity of the stabilizing cap localized at the growing microtubule tip (70). While this is the first time CLASP2 and G2L1 have been observed to shift in real-time after insulin stimulation from predominant plus-end localization to trailing along the growing length of the microtubule, it is not the first time an alteration in the spatial relationship between CLASP2 and microtubules has been captured. In live migrating Ptk1 epithelial cells, within the cell body, CLASP2 displayed typical +TIP action, whereas lamella and lamellipodium-based CLASP2 lacked +TIP behaviour and instead exhibited trailing via binding along the length of the growing microtubule lattice (52), very reminiscent of the effect of insulin we observed. As Wittmann and Waterman-Storer stated (52), CLASP2 shifts from true +TIP behaviour to full lattice decoration, a style of microtubule association more reminiscent of classic MAP family members (8). Hypothetically, these newly created microtubules populated with lattice dispersion of CLASP2 and G2L1 trails may serve as a signal to assemble or initiate an as-of-yet undetermined molecular event, in this case, a signalling signature associated with insulin action. There is noticeable heterogeneity in the literature with regards to findings on CLASP2 movement, which can be explained in part by the fact that different cell types possess alternative proteomes, and these differences probably influence the cooperative nature (49) and resulting behaviour of +TIPs. For example, the spatio-temporal changes in CLASP2 reported for wound healing experiments in Ptk1 epithelial cells (52) and HaCat keratinocytes (16) were not observed in motile 3T3 fibroblasts,

although, when the 3T3 fibroblasts underwent serum stimulation, CLASP2 accumulated and immobilized at the leading edge of the cell in yet another pattern of localization (10, 14, 72). These different phenotypes are distinct from the population of CLASP2 that has been observed at the Golgi (73, 74). So, overall, there is support for a diverse range of CLASP2 regulation and function that can be dictated by multiple aspects, including cell-specific needs and intracellular localization.

This insulin-stimulated +TIP trailing along newly created microtubules possessed what we viewed as a "brace-like" appearance, and since prior studies support a microtubule-stabilizing role for CLASP2 (10, 69, 70), we hypothesized that insulin stimulates the stabilization of selective microtubules. Follow-up studies discovered that insulin stimulates α-tubulin Lysine 40 acetylation ("AcK40"), a post-translational modification within the 15-nm-wide lumen of the microtubule that is associated with stabilization of both long-lived and curved microtubules (50, 51, 75). AcK40 only occurs on polymerized microtubules (76-79) and is catalysed by the tubulin acetyltransferase aTAT1 (80, 81) whereas the exclusively cytoplasmic (82) histone deacetylase 6 (HDAC6) deacetylates tubulin (83). AcK40 takes place on polymerized microtubules to reduce structural strain by increasing microtubule flexibility (50, 51). These stabilized microtubules, by becoming protected against breaking and shrinkage, exist for prolonged periods of time (77, 78, 84). Insulin-stimulated CLASP2/G2L1 trailing occurred acutely, within minutes of insulin treatment, whereas the effect of insulin on microtubule stabilization via AcK40 was gradual, indicating that trailing events precede stabilization, although whether a causal relationship exists between +TIP trailing and microtubule stabilization is unknown and whether trailing and AcK40 occur on the same microtubules will be the subject of future studies. Since the effect of insulin on AcK40 was not rapid (as seen with Akt substrates (85)) but was instead delayed and profiled more like the effects of insulin observed for mTOR substrates (85), we tested and confirmed that inhibition of mTOR with rapamycin blocks insulin-stimulated AcK40. The control of insulin-stimulated AcK40 by mTOR was found to be counterbalanced by GSK3-mediated suppression of AcK40 in the basal

state. Future studies will be aimed at testing the hypothesis that, through insulin-mediated suppression of GSK3 activity and activation of mTOR, insulin influences HDAC6 and aTAT1 activity to control α-tubulin AcK40 (modelled in Figure 7I).

Of all of the microtubule-regulating protein interactome studies we have completed thus far using the label-free spectrum counting technique we have devised, none of the validated network proteins analyzed have exhibited measureable protein abundance changes after insulin-stimulation. In this report, our traditional co-IP and western blot confirmatory follow-up experiments led to findings that agreed with the quantitative proteomics data, the proteins did in fact co-IP although the abundance of the co-immunoprecipitated proteins was not reproducibly affected by insulin. As an alternative to changes in protein association, we hypothesized that since CLASP2 undergoes robust insulin-stimulated phosphorylation (11), perhaps the 3T3-L1 adipocyte CLASP2 protein network proteins serve as potential candidates for insulin-regulated phosphorylation. We developed a straight-forward approach to quantifying changes in protein phosphorylation that incorporated basic immunoprecipitation and in-gel protein digestion techniques together with automated label-free quantification of extracted ion abundance performed in the software program Progenesis QI for Proteomics. This protein-specific quantitative phosphoproteomics approach expanded the number of +TIPs known to undergo insulin-regulated phosphorylation from just CLASP2 to a list that now includes CLIP2, G2L1, EB1 and CKAP5, while we also discovered that the CLASP2 network members MARK2 and AGAP3 undergo insulin-regulated phosphorylation as well (hypothetically modelled in Figure 1C). Of all the sites analyzed, the phosphorylation of CLIP2 (also known as CLIP-115) at Ser552 underwent the strongest increase upon insulin treatment. Phosphorylation of CLIP1 (also known as CLIP-170) at Thr287 and Ser195/Ser1318 has been linked to centrosome duplication and kinetochore-microtubule attachments (86, 87), respectively, although Ser1318 of CLIP1 is not found in the shorter CLIP2 isoform, while Ser552, the insulin-stimulated phosphorylation site of CLIP2, is not

conserved in CLIP1. Ser552 lies approximately 300 amino acids past the second microtubule-binding Cytoskeleton-associated protein Gly-rich ("CAP-Gly") domain (88) and the surrounding serine-rich basic regions within the N-terminus of CLIP2 and is positioned along the extensive coiled-coil region of CLIP2 known to mediate CLIP2 dimerization (89). CLIP1 and CLIP2 association with microtubules has been shown to be regulated by phosphorylation in a negative manner (89-91). Phosphorylation also regulates CLIP1 intramolecular association and accompanying CLIP1 conformational changes (92). Each of these phospho-regulated events has been linked to phosphorylation sites near the CAP-GLY domains and the surrounding serine-rich basic regions within the N-terminus of the CLIPs, rendering the insulin-stimulated Ser552 CLIP2 phosphorylation site with the potential to be functionally distinct. The CLASP2 interactome project revealed a novel association between the +TIP CLIP2 and the GTPase-activating proteins AGAP1 and AGAP3 (24). There is a key difference between the CLASP2/G2L1 interaction and the proposed complex between CLIP2 and the AGAPs, in that the AGAPs are the lone protein members of the CLASP2 network in 3T3-L1 adipocytes that act as both a GTPase (93, 94) and a GTPase activating protein (95, 96). In addition, the AGAPs also contain a Pleckstrin Homology ("PH") domain, whose known functions include mediating protein-protein interactions as well as membrane localization through the binding of phosphoinositides (97). Of the insulin-stimulated AGAP3 phosphorylation sites we have discovered, one is within the GTPase domain (pSer300) while the other is located within the PH domain (pSer478). CLIP2 was the most enriched protein in the AGAP3 interactome (24), supportive of the hypothesis that functional cooperativity exists between CLIP2 and AGAP3 in the context of insulin action.

EB1, known as "the master integrator of +TIP networks" (49) as well as CKAP5 (alternatively referred to as ch-TOG) (56, 98), also undergo insulin-regulated phosphorylation. EB1, like CLASP2, G2L1, and CLIP2, tracks growing microtubule plus-ends and acts as an integrating scaffold protein that promotes a wide variety of +TIP localization to the growing

microtubule plus-end (99). Phosphorylation of EB proteins is known to regulate microtubule dynamics and EB function in a variety of organisms and biological systems (100-109). The insulin-stimulated EB1 phosphorylation site we detected, Ser155, lies in the coiled-coil linker region of EB1 that bridges the N-terminal Calponin-homology (CH) domain to the C-terminal EB homology (EBH) domain and adjacent EEY/F motif. Ser155 of EB1 already has a possible connection with major players in insulin action, as AKT and GSK3 regulate levels of Ser155 phosphorylation to control EB1 localization to microtubule plus-ends (110). CKAP5 is a member of the XMAP215 family of microtubule polymerases that catalyzes the addition of tubulin dimers to elongating microtubule plus-ends. CKAP5 localizes to the extreme tip of the growing microtubule plus end whereas EB1 is further down the microtubule (111), so in an *in vitro* model for example, EB1 is located tens of nanometers further down the microtubule from CKAP5 (112). CKAP5 consists of five successive TOG domains that span across the majority of this 225kDa protein while a microtubule lattice binding domain is located between the fourth and fifth TOG domains, all of which participate in the processive addition of tubulin dimers to the growing microtubule plus end (113, 114). Within the CKAP5 C-terminus lies both a cryptic TOG domain as well as a shorter four α-helix-based domain (with no known identity) that mediates protein-protein interactions (115, 116). It is within this terminal multi-α-helix-containing domain where insulin significantly affects the phosphorylation of CKAP5 at Ser1861 in a suppressive manner. We discovered a stretch of CKAP5 phosphorylation sites spanning amino acids 1800-1870 that also trend towards insulin-mediated suppression of phosphorylation (Supplemental Figure 2F), although the four biological replicates analysed did not achieve statistical significance. With CKAP5 playing such a vital role in cytoskeletal management, it is of future interest to elucidate the significance of insulin-mediated changes in CKAP5 phosphorylation within the context of insulin-controlled microtubule dynamics.

Another protein we discovered to undergo insulin-regulated phosphorylation was the only kinase of the group, MARK2 (also known as Par-1b). Classical MAPs bind and release along the

microtubule lattice as a mode of microtubule regulation, a process that is controlled in part by transient MAP phosphorylation by the MARK family kinases (reviewed in (8)). MARK2-mediated release of the various MAPs from the microtubule lattice affects the stabilization of microtubules, microtubule polymerization, microtubule bundling, the association between microtubules and actin, and microtubule mediated motor transport of intracellular cargo (8). Insulin stimulates an increase in the phosphorylation of MARK2 at Ser40, Thr42 and Ser43, a short stretch of residues that lies adjacent to the MARK2 kinase domain, while phosphorylation within the spacer region of MARK2 at Ser568 undergoes insulin-mediated suppression. MARK2 makes an intriguing hypothetical candidate kinase for insulin regulation since so many MAPs are under MARK2 control and MAPs are a critical component for fine-tuning microtubule dynamics.

The novel findings we present significantly expand the number of known +TIPs affected by insulin form a new hypothesis that a network of proteins linked to microtubule regulation synergize to coordinate insulin-regulated MT dynamics. Upon initial investigation of the effect of insulin on two of these network proteins, CLASP2 and G2L1, we discovered +TIP trailing, a new mode of insulin-regulated protein behaviour. Follow-up studies determined that insulin stimulates α-tubulin Lysine 40 acetylation, a discovery that led to the finding that insulin increases microtubule stabilization. Taken together, we have expanded the protein systems and cytoskeletal elements involved in insulin action, information that is paramount for developing future studies aimed at understanding and identifying underlying mechanisms of insulin resistance, a hallmark of type 2 diabetes.

REFERENCES

1. Ridley, A. J., Paterson, H. F., Johnston, C. L., Diekmann, D., and Hall, A. (1992) The small GTP-binding protein rac regulates growth factor-induced membrane ruffling. *Cell* 70, 401-410

2. Semiz, S., Park, J. G., Nicoloro, S. M., Furcinitti, P., Zhang, C., Chawla, A., Leszyk, J., and Czech, M. P. (2003) Conventional kinesin KIF5B mediates insulin-stimulated GLUT4 movements on microtubules. *EMBO J* 22, 2387-2399

3. Koumanov, F., Jin, B., Yang, J., and Holman, G. D. (2005) Insulin signaling meets vesicle traffic of GLUT4 at a plasma-membrane-activated fusion step. *Cell Metab* 2, 179-189

4. Kanzaki, M., and Pessin, J. E. (2001) Insulin-stimulated GLUT4 translocation in adipocytes is dependent upon cortical actin remodeling. *J Biol Chem* 276, 42436-42444

5. Tong, P., Khayat, Z. A., Huang, C., Patel, N., Ueyama, A., and Klip, A. (2001) Insulin-induced cortical actin remodeling promotes GLUT4 insertion at muscle cell membrane ruffles. *J Clin Invest* 108, 371-381

6. Jiang, Z. Y., Chawla, A., Bose, A., Way, M., and Czech, M. P. (2002) A phosphatidylinositol 3-kinase-independent insulin signaling pathway to N-WASP/Arp2/3/F-actin required for GLUT4 glucose transporter recycling. *J Biol Chem* 277, 509-515

7. Chiu, T. T., Jensen, T. E., Sylow, L., Richter, E. A., and Klip, A. (2011) Rac1 signalling towards GLUT4/glucose uptake in skeletal muscle. *Cell Signal* 23, 1546-1554

8. Ramkumar, A., Jong, B. Y., and Ori-McKenney, K. M. (2018) ReMAPping the microtubule landscape: How phosphorylation dictates the activities of microtubule-associated proteins. *Dev Dyn* 247, 138-155

9. Galjart, N. (2010) Plus-end-tracking proteins and their interactions at microtubule ends. *Curr Biol* 20, R528-537

10. Akhmanova, A., Hoogenraad, C. C., Drabek, K., Stepanova, T., Dortland, B., Verkerk, T., Vermeulen, W., Burgering, B. M., De Zeeuw, C. I., Grosveld, F., and Galjart, N. (2001) Clasps are CLIP-115 and -170 associating proteins involved in the regional regulation of microtubule dynamics in motile fibroblasts. *Cell* 104, 923-935

11. Langlais, P., Dillon, J. L., Mengos, A., Baluch, D. P., Ardebili, R., Miranda, D. N., Xie, X., Heckmann, B. L., Liu, J., and Mandarino, L. J. (2012) Identification of a role for CLASP2 in insulin action. *J Biol Chem* 287, 39245-39253

12. Galjart, N. (2005) CLIPs and CLASPs and cellular dynamics. *Nat Rev Mol Cell Biol* 6, 487-498

13. Mitchison, T., Evans, L., Schulze, E., and Kirschner, M. (1986) Sites of microtubule assembly and disassembly in the mitotic spindle. *Cell* 45, 515-527

14. Lansbergen, G., Grigoriev, I., Mimori-Kiyosue, Y., Ohtsuka, T., Higa, S., Kitajima, I., Demmers, J., Galjart, N., Houtsmuller, A. B., Grosveld, F., and Akhmanova, A. (2006) CLASPs attach microtubule plus ends to the cell cortex through a complex with LL5beta. *Dev Cell* 11, 21-32

15. Noordstra, I., and Akhmanova, A. (2017) Linking cortical microtubule attachment and exocytosis. *F1000Res* 6, 469

16. Kumar, P., Lyle, K. S., Gierke, S., Matov, A., Danuser, G., and Wittmann, T. (2009) GSK3beta phosphorylation modulates CLASP-microtubule association and lamella microtubule attachment. *J Cell Biol* 184, 895-908

17. Mimori-Kiyosue, Y., Grigoriev, I., Lansbergen, G., Sasaki, H., Matsui, C., Severin, F., Galjart, N., Grosveld, F., Vorobjev, I., Tsukita, S., and Akhmanova, A. (2005) CLASP1 and CLASP2 bind to EB1 and regulate microtubule plus-end dynamics at the cell cortex. *J Cell Biol* 168, 141-153

18. Ruiz-Saenz, A., van Haren, J., Laura Sayas, C., Rangel, L., Demmers, J., Millan, J., Alonso, M. A., Galjart, N., and Correas, I. (2013) Protein 4.1R binds to CLASP2 and regulates dynamics, organization and attachment of microtubules to the cell cortex. *J Cell Sci* 126, 4589-4601

19. Basu, S., Sladecek, S., Martinez de la Pena y Valenzuela, I., Akaaboune, M., Smal, I., Martin, K., Galjart, N., and Brenner, H. R. (2015) CLASP2-dependent microtubule capture at the neuromuscular junction membrane requires LL5beta and actin for focal delivery of acetylcholine receptor vesicles. *Mol Biol Cell* 26, 938-951

20. Stehbens, S. J., Paszek, M., Pemble, H., Ettinger, A., Gierke, S., and Wittmann, T. (2014) CLASPs link focal-adhesion-associated microtubule capture to localized exocytosis and adhesion site turnover. *Nat Cell Biol* 16, 561-573

21. Bartolini, F., and Gundersen, G. G. (2010) Formins and microtubules. *Biochim Biophys Acta* 1803, 164-173

22. Zhang, J., Yue, J., and Wu, X. (2017) Spectraplakin family proteins - cytoskeletal crosslinkers with versatile roles. *J Cell Sci* 130, 2447-2457

23. Stroud, M. J., Nazgiewicz, A., McKenzie, E. A., Wang, Y., Kammerer, R. A., and Ballestrem, C. (2014) GAS2-like proteins mediate communication between microtubules and actin through interactions with end-binding proteins. *J Cell Sci* 127, 2672-2682

24. Kruse, R., Krantz, J., Barker, N., Coletta, R. L., Rafikov, R., Luo, M., Hojlund, K., Mandarino, L. J., and Langlais, P. R. (2017) Characterization of the CLASP2 Protein Interaction Network Identifies SOGA1 as a Microtubule-Associated Protein. *Mol Cell Proteomics* 16, 1718-1735

25. Goriounov, D., Leung, C. L., and Liem, R. K. (2003) Protein products of human Gas2-related genes on chromosomes 17 and 22 (hGAR17 and hGAR22) associate with both microfilaments and microtubules. *J Cell Sci* 116, 1045-1058

26. Jiang, K., Toedt, G., Montenegro Gouveia, S., Davey, N. E., Hua, S., van der Vaart, B., Grigoriev, I., Larsen, J., Pedersen, L. B., Bezstarosti, K., Lince-Faria, M., Demmers, J., Steinmetz, M. O., Gibson, T. J., and Akhmanova, A. (2012) A Proteome-wide screen for mammalian SxIP motif-containing microtubule plus-end tracking proteins. *Curr Biol* 22, 1800-1807

27. Talior-Volodarsky, I., Randhawa, V. K., Zaid, H., and Klip, A. (2008) Alpha-actinin-4 is selectively required for insulin-induced GLUT4 translocation. *J Biol Chem* 283, 25115-25123

28. Olson, A. L., Eyster, C. A., Duggins, Q. S., and Knight, J. B. (2003) Insulin promotes formation of polymerized microtubules by a phosphatidylinositol 3-kinase-independent, actin-dependent pathway in 3T3-L1 adipocytes. *Endocrinology* 144, 5030-5039

29. Dawicki-McKenna, J. M., Goldman, Y. E., and Ostap, E. M. (2012) Sites of glucose transporter-4 vesicle fusion with the plasma membrane correlate spatially with microtubules. *PLoS One* 7, e43662

30. Chambers, M. C., Maclean, B., Burke, R., Amodei, D., Ruderman, D. L., Neumann, S., Gatto, L., Fischer, B., Pratt, B., Egertson, J., Hoff, K., Kessner, D., Tasman, N., Shulman, N., Frewen, B., Baker, T. A., Brusniak, M. Y., Paulse, C., Creasy, D., Flashner, L., Kani, K., Moulding, C., Seymour, S. L., Nuwaysir, L. M., Lefebvre, B., Kuhlmann, F., Roark, J., Rainer, P., Detlev, S.,

Hemenway, T., Huhmer, A., Langridge, J., Connolly, B., Chadick, T., Holly, K., Eckels, J., Deutsch, E. W., Moritz, R. L., Katz, J. E., Agus, D. B., MacCoss, M., Tabb, D. L., and Mallick, P. (2012) A cross-platform toolkit for mass spectrometry and proteomics. *Nat Biotechnol* 30, 918-920

31. Vizcaino, J. A., Cote, R. G., Csordas, A., Dianes, J. A., Fabregat, A., Foster, J. M., Griss, J., Alpi, E., Birim, M., Contell, J., O'Kelly, G., Schoenegger, A., Ovelleiro, D., Perez-Riverol, Y., Reisinger, F., Rios, D., Wang, R., and Hermjakob, H. (2013) The PRoteomics IDEntifications (PRIDE) database and associated tools: status in 2013. *Nucleic Acids Res* 41, D1063-1069

32. Langlais, P., Mandarino, L. J., and Yi, Z. (2010) Label-free relative quantification of co-eluting isobaric phosphopeptides of insulin receptor substrate-1 by HPLC-ESI-MS/MS. *J Am Soc Mass Spectrom* 21, 1490-1499

33. Langlais, P., Yi, Z., Finlayson, J., Luo, M., Mapes, R., De Filippis, E., Meyer, C., Plummer, E., Tongchinsub, P., Mattern, M., and Mandarino, L. J. (2011) Global IRS-1 phosphorylation analysis in insulin resistance. *Diabetologia* 54, 2878-2889

34. Langlais, P., Yi, Z., and Mandarino, L. J. (2011) The identification of raptor as a substrate for p44/42 MAPK. *Endocrinology* 152, 1264-1273

35. Padilla-Rodriguez, M., Parker, S. S., Adams, D. G., Westerling, T., Puleo, J. I., Watson, A. W., Hill, S. M., Noon, M., Gaudin, R., Aaron, J., Tong, D., Roe, D. J., Knudsen, B., and Mouneimne, G. (2018) The actin cytoskeletal architecture of estrogen receptor positive breast cancer cells suppresses invasion. *Nat Commun* 9, 2980

36. Schindelin, J., Arganda-Carreras, I., Frise, E., Kaynig, V., Longair, M., Pietzsch, T., Preibisch, S., Rueden, C., Saalfeld, S., Schmid, B., Tinevez, J. Y., White, D. J., Hartenstein, V.,

Eliceiri, K., Tomancak, P., and Cardona, A. (2012) Fiji: an open-source platform for biological-image analysis. *Nat Methods* 9, 676-682

37. Longair, M. H., Baker, D. A., and Armstrong, J. D. (2011) Simple Neurite Tracer: open source software for reconstruction, visualization and analysis of neuronal processes. *Bioinformatics* 27, 2453-2454

38. Shah, N., Kumar, S., Zaman, N., Pan, C. C., Bloodworth, J. C., Lei, W., Streicher, J. M., Hempel, N., Mythreye, K., and Lee, N. Y. (2018) TAK1 activation of alpha-TAT1 and microtubule hyperacetylation control AKT signaling and cell growth. *Nat Commun* 9, 1696

39. Yi, Z., Langlais, P., De Filippis, E. A., Luo, M., Flynn, C. R., Schroeder, S., Weintraub, S. T., Mapes, R., and Mandarino, L. J. (2007) Global assessment of regulation of phosphorylation of insulin receptor substrate-1 by insulin in vivo in human muscle. *Diabetes* 56, 1508-1516

40. Kumar, P., and Wittmann, T. (2012) +TIPs: SxIPping along microtubule ends. *Trends Cell Biol* 22, 418-428

41. Choi, H., Glatter, T., Gstaiger, M., and Nesvizhskii, A. I. (2012) SAINT-MS1: protein-protein interaction scoring using label-free intensity data in affinity purification-mass spectrometry experiments. *J Proteome Res* 11, 2619-2624

42. Choi, H., Larsen, B., Lin, Z. Y., Breitkreutz, A., Mellacheruvu, D., Fermin, D., Qin, Z. S., Tyers, M., Gingras, A. C., and Nesvizhskii, A. I. (2011) SAINT: probabilistic scoring of affinity purification-mass spectrometry data. *Nat Methods* 8, 70-73

43. Choi, H., Liu, G., Mellacheruvu, D., Tyers, M., Gingras, A. C., and Nesvizhskii, A. I. (2012) Analyzing protein-protein interactions from affinity purification-mass spectrometry data with SAINT. *Curr Protoc Bioinformatics* Chapter 8, Unit8 15

44. Shannon, P., Markiel, A., Ozier, O., Baliga, N. S., Wang, J. T., Ramage, D., Amin, N., Schwikowski, B., and Ideker, T. (2003) Cytoscape: a software environment for integrated models of biomolecular interaction networks. *Genome Res* 13, 2498-2504

45. Morris, J. H., Knudsen, G. M., Verschueren, E., Johnson, J. R., Cimermancic, P., Greninger, A. L., and Pico, A. R. (2014) Affinity purification-mass spectrometry and network analysis to understand protein-protein interactions. *Nat Protoc* 9, 2539-2554

46. Westermarck, J., Ivaska, J., and Corthals, G. L. (2013) Identification of protein interactions involved in cellular signaling. *Mol Cell Proteomics* 12, 1752-1763

47. Jin, L., Williamson, A., Banerjee, S., Philipp, I., and Rape, M. (2008) Mechanism of ubiquitin-chain formation by the human anaphase-promoting complex. *Cell* 133, 653-665

48. Loo, L. H., Lin, H. J., Singh, D. K., Lyons, K. M., Altschuler, S. J., and Wu, L. F. (2009) Heterogeneity in the physiological states and pharmacological responses of differentiating 3T3-L1 preadipocytes. *J Cell Biol* 187, 375-384

49. Akhmanova, A., and Steinmetz, M. O. (2015) Control of microtubule organization and dynamics: two ends in the limelight. *Nat Rev Mol Cell Biol* 16, 711-726

50. Portran, D., Schaedel, L., Xu, Z., Thery, M., and Nachury, M. V. (2017) Tubulin acetylation protects long-lived microtubules against mechanical ageing. *Nat Cell Biol* 19, 391-398

51. Xu, Z., Schaedel, L., Portran, D., Aguilar, A., Gaillard, J., Marinkovich, M. P., Thery, M., and Nachury, M. V. (2017) Microtubules acquire resistance from mechanical breakage through intralumenal acetylation. *Science* 356, 328-332

52. Wittmann, T., and Waterman-Storer, C. M. (2005) Spatial regulation of CLASP affinity for microtubules by Rac1 and GSK3beta in migrating epithelial cells. *J Cell Biol* 169, 929-939

53. Grimaldi, A. D., Maki, T., Fitton, B. P., Roth, D., Yampolsky, D., Davidson, M. W., Svitkina, T., Straube, A., Hayashi, I., and Kaverina, I. (2014) CLASPs are required for proper microtubule localization of end-binding proteins. *Dev Cell* 30, 343-352

54. Gupta, K. K., Alberico, E. O., Nathke, I. S., and Goodson, H. V. (2014) Promoting microtubule assembly: A hypothesis for the functional significance of the +TIP network. *Bioessays* 36, 818-826

55. Tamura, N., and Draviam, V. M. (2012) Microtubule plus-ends within a mitotic cell are 'moving platforms' with anchoring, signalling and force-coupling roles. *Open Biol* 2, 120132

56. Al-Bassam, J., and Chang, F. (2011) Regulation of microtubule dynamics by TOG-domain proteins XMAP215/Dis1 and CLASP. *Trends Cell Biol* 21, 604-614

57. Gamper, I., Fleck, D., Barlin, M., Spehr, M., El Sayad, S., Kleine, H., Maxeiner, S., Schalla, C., Aydin, G., Hoss, M., Litchfield, D. W., Luscher, B., Zenke, M., and Sechi, A. (2016) GAR22beta regulates cell migration, sperm motility, and axoneme structure. *Mol Biol Cell* 27, 277-294

58. Gamper, I., Koh, K. R., Ruau, D., Ullrich, K., Bartunkova, J., Piroth, D., Hacker, C., Bartunek, P., and Zenke, M. (2009) GAR22: a novel target gene of thyroid hormone receptor causes growth inhibition in human erythroid cells. *Exp Hematol* 37, 539-548 e534

59. Maiato, H., Fairley, E. A., Rieder, C. L., Swedlow, J. R., Sunkel, C. E., and Earnshaw, W. C. (2003) Human CLASP1 is an outer kinetochore component that regulates spindle microtubule dynamics. *Cell* 113, 891-904

60. Maiato, H., Khodjakov, A., and Rieder, C. L. (2005) Drosophila CLASP is required for the incorporation of microtubule subunits into fluxing kinetochore fibres. *Nat Cell Biol* 7, 42-47

61. Bratman, S. V., and Chang, F. (2007) Stabilization of overlapping microtubules by fission yeast CLASP. *Dev Cell* 13, 812-827

62. Sousa, A., Reis, R., Sampaio, P., and Sunkel, C. E. (2007) The Drosophila CLASP homologue, Mast/Orbit regulates the dynamic behaviour of interphase microtubules by promoting the pause state. *Cell Motil Cytoskeleton* 64, 605-620

63. Maton, G., Edwards, F., Lacroix, B., Stefanutti, M., Laband, K., Lieury, T., Kim, T., Espeut, J., Canman, J. C., and Dumont, J. (2015) Kinetochore components are required for central spindle assembly. *Nat Cell Biol* 17, 697-705

64. Lacroix, B., Bourdages, K. G., Dorn, J. F., Ihara, S., Sherwood, D. R., Maddox, P. S., and Maddox, A. S. (2014) In situ imaging in C. elegans reveals developmental regulation of microtubule dynamics. *Dev Cell* 29, 203-216

65. Ambrose, C., Allard, J. F., Cytrynbaum, E. N., and Wasteneys, G. O. (2011) A CLASP-modulated cell edge barrier mechanism drives cell-wide cortical microtubule organization in Arabidopsis. *Nat Commun* 2, 430

66. Bouchet, B. P., Noordstra, I., van Amersfoort, M., Katrukha, E. A., Ammon, Y. C., Ter Hoeve, N. D., Hodgson, L., Dogterom, M., Derksen, P. W. B., and Akhmanova, A. (2016) Mesenchymal Cell Invasion Requires Cooperative Regulation of Persistent Microtubule Growth by SLAIN2 and CLASP1. *Dev Cell* 39, 708-723

67. Moriwaki, T., and Goshima, G. (2016) Five factors can reconstitute all three phases of microtubule polymerization dynamics. *Journal of Cell Biology* 215, 357-368

68. Yu, N., Signorile, L., Basu, S., Ottema, S., Lebbink, J. H. G., Leslie, K., Smal, I., Dekkers, D., Demmers, J., and Galjart, N. (2016) Isolation of Functional Tubulin Dimers and of Tubulin-Associated Proteins from Mammalian Cells. *Curr Biol* 26, 1728-1736

69. Lawrence, E. J., Arpag, G., Norris, S. R., and Zanic, M. (2018) Human CLASP2 specifically regulates microtubule catastrophe and rescue. *Mol Biol Cell* 29, 1168-1177

70. Aher, A., Kok, M., Sharma, A., Rai, A., Olieric, N., Rodriguez-Garcia, R., Katrukha, E. A., Weinert, T., Olieric, V., Kapitein, L. C., Steinmetz, M. O., Dogterom, M., and Akhmanova, A. (2018) CLASP Suppresses Microtubule Catastrophes through a Single TOG Domain. *Dev Cell* 46, 40-58 e48

71. Patel, K., Nogales, E., and Heald, R. (2012) Multiple domains of human CLASP contribute to microtubule dynamics and organization in vitro and in Xenopus egg extracts. *Cytoskeleton (Hoboken)* 69, 155-165

72. Drabek, K., van Ham, M., Stepanova, T., Draegestein, K., van Horssen, R., Sayas, C. L., Akhmanova, A., Ten Hagen, T., Smits, R., Fodde, R., Grosveld, F., and Galjart, N. (2006) Role of CLASP2 in microtubule stabilization and the regulation of persistent motility. *Curr Biol* 16, 2259-2264

73. Efimov, A., Kharitonov, A., Efimova, N., Loncarek, J., Miller, P. M., Andreyeva, N., Gleeson, P., Galjart, N., Maia, A. R., McLeod, I. X., Yates, J. R., 3rd, Maiato, H., Khodjakov, A., Akhmanova, A., and Kaverina, I. (2007) Asymmetric CLASP-dependent nucleation of noncentrosomal microtubules at the trans-Golgi network. *Dev Cell* 12, 917-930

74. Miller, P. M., Folkmann, A. W., Maia, A. R., Efimova, N., Efimov, A., and Kaverina, I. (2009) Golgi-derived CLASP-dependent microtubules control Golgi organization and polarized trafficking in motile cells. *Nat Cell Biol* 11, 1069-1080

75. Janke, C., and Montagnac, G. (2017) Causes and Consequences of Microtubule Acetylation. *Curr Biol* 27, R1287-R1292

76. L'Hernault, S. W., and Rosenbaum, J. L. (1983) Chlamydomonas alpha-tubulin is posttranslationally modified in the flagella during flagellar assembly. *J Cell Biol* 97, 258-263

77. Maruta, H., Greer, K., and Rosenbaum, J. L. (1986) The acetylation of alpha-tubulin and its relationship to the assembly and disassembly of microtubules. *J Cell Biol* 103, 571-579

78. Piperno, G., LeDizet, M., and Chang, X. J. (1987) Microtubules containing acetylated alpha-tubulin in mammalian cells in culture. *J Cell Biol* 104, 289-302

79. Bulinski, J. C., Richards, J. E., and Piperno, G. (1988) Posttranslational modifications of alpha tubulin: detyrosination and acetylation differentiate populations of interphase microtubules in cultured cells. *J Cell Biol* 106, 1213-1220

80. Akella, J. S., Wloga, D., Kim, J., Starostina, N. G., Lyons-Abbott, S., Morrissette, N. S., Dougan, S. T., Kipreos, E. T., and Gaertig, J. (2010) MEC-17 is an alpha-tubulin acetyltransferase. *Nature* 467, 218-222

81. Shida, T., Cueva, J. G., Xu, Z., Goodman, M. B., and Nachury, M. V. (2010) The major alpha-tubulin K40 acetyltransferase alphaTAT1 promotes rapid ciliogenesis and efficient mechanosensation. *Proc Natl Acad Sci U S A* 107, 21517-21522

82. Verdel, A., Curtet, S., Brocard, M. P., Rousseaux, S., Lemercier, C., Yoshida, M., and Khochbin, S. (2000) Active maintenance of mHDA2/mHDAC6 histone-deacetylase in the cytoplasm. *Curr Biol* 10, 747-749

83. Hubbert, C., Guardiola, A., Shao, R., Kawaguchi, Y., Ito, A., Nixon, A., Yoshida, M., Wang, X. F., and Yao, T. P. (2002) HDAC6 is a microtubule-associated deacetylase. *Nature* 417, 455-458

84. LeDizet, M., and Piperno, G. (1986) Cytoplasmic microtubules containing acetylated alpha-tubulin in Chlamydomonas reinhardtii: spatial arrangement and properties. *J Cell Biol* 103, 13-22

85. Humphrey, S. J., Yang, G., Yang, P., Fazakerley, D. J., Stockli, J., Yang, J. Y., and James, D. E. (2013) Dynamic adipocyte phosphoproteome reveals that Akt directly regulates mTORC2. *Cell Metab* 17, 1009-1020

86. Li, H. C., Liu, X. S., Yang, X. M., Wang, Y. M., Wang, Y., Turner, J. R., and Liu, X. Q. (2010) Phosphorylation of CLIP-170 by Plk1 and CK2 promotes timely formation of kinetochore-microtubule attachments. *Embo Journal* 29, 2953-2965

87. Yang, X., Li, H., Liu, X. S., Deng, A., and Liu, X. (2009) Cdc2-mediated phosphorylation of CLIP-170 is essential for its inhibition of centrosome reduplication. *J Biol Chem* 284, 28775-28782

88. Lansbergen, G., Komarova, Y., Modesti, M., Wyman, C., Hoogenraad, C. C., Goodson, H. V., Lemaitre, R. P., Drechsel, D. N., van Munster, E., Gadella, T. W., Jr., Grosveld, F., Galjart, N., Borisy, G. G., and Akhmanova, A. (2004) Conformational changes in CLIP-170 regulate its binding to microtubules and dynactin localization. *J Cell Biol* 166, 1003-1014

89. Hoogenraad, C. C., Akhmanova, A., Grosveld, F., De Zeeuw, C. I., and Galjart, N. (2000) Functional analysis of CLIP-115 and its binding to microtubules. *J Cell Sci* 113 (Pt 12), 2285-2297

90. Rickard, J. E., and Kreis, T. E. (1991) Binding of pp170 to microtubules is regulated by phosphorylation. *J Biol Chem* 266, 17597-17605

91. Choi, J. H., Bertram, P. G., Drenan, R., Carvalho, J., Zhou, H. H., and Zheng, X. F. (2002) The FKBP12-rapamycin-associated protein (FRAP) is a CLIP-170 kinase. *EMBO Rep* 3, 988-994

92. Lee, H. S., Komarova, Y. A., Nadezhdina, E. S., Anjum, R., Peloquin, J. G., Schober, J. M., Danciu, O., van Haren, J., Galjart, N., Gygi, S. P., Akhmanova, A., and Borisy, G. G. (2010) Phosphorylation controls autoinhibition of cytoplasmic linker protein-170. *Mol Biol Cell* 21, 2661-2673

93. Soundararajan, M., Yang, X., Elkins, J. M., Sobott, F., and Doyle, D. A. (2007) The centaurin gamma-1 GTPase-like domain functions as an NTPase. *Biochem J* 401, 679-688

94. Xia, C., Ma, W., Stafford, L. J., Liu, C., Gong, L., Martin, J. F., and Liu, M. (2003) GGAPs, a new family of bifunctional GTP-binding and GTPase-activating proteins. *Mol Cell Biol* 23, 2476-2488

95. Nie, Z., Stanley, K. T., Stauffer, S., Jacques, K. M., Hirsch, D. S., Takei, J., and Randazzo, P. A. (2002) AGAP1, an endosome-associated, phosphoinositide-dependent ADP-ribosylation factor GTPase-activating protein that affects actin cytoskeleton. *J Biol Chem* 277, 48965-48975

96. Luo, R., Akpan, I. O., Hayashi, R., Sramko, M., Barr, V., Shiba, Y., and Randazzo, P. A. (2012) GTP-binding protein-like domain of AGAP1 is protein binding site that allosterically regulates ArfGAP protein catalytic activity. *J Biol Chem* 287, 17176-17185

97. Halet, G. (2005) Imaging phosphoinositide dynamics using GFP-tagged protein domains. *Biol Cell* 97, 501-518

98. Brouhard, G. J., Stear, J. H., Noetzel, T. L., Al-Bassam, J., Kinoshita, K., Harrison, S. C., Howard, J., and Hyman, A. A. (2008) XMAP215 is a processive microtubule polymerase. *Cell* 132, 79-88

99. Nehlig, A., Molina, A., Rodrigues-Ferreira, S., Honore, S., and Nahmias, C. (2017) Regulation of end-binding protein EB1 in the control of microtubule dynamics. *Cell Mol Life Sci* 74, 2381-2393

100. Zimniak, T., Stengl, K., Mechtler, K., and Westermann, S. (2009) Phosphoregulation of the budding yeast EB1 homologue Bim1p by Aurora/Ipl1p. *J Cell Biol* 186, 379-391

101. Iimori, M., Ozaki, K., Chikashige, Y., Habu, T., Hiraoka, Y., Maki, T., Hayashi, I., Obuse, C., and Matsumoto, T. (2012) A mutation of the fission yeast EB1 overcomes negative regulation by phosphorylation and stabilizes microtubules. *Exp Cell Res* 318, 262-275

102. Ban, R., Matsuzaki, H., Akashi, T., Sakashita, G., Taniguchi, H., Park, S. Y., Tanaka, H., Furukawa, K., and Urano, T. (2009) Mitotic regulation of the stability of microtubule plus-end tracking protein EB3 by ubiquitin ligase SIAH-1 and Aurora mitotic kinases. *J Biol Chem* 284, 28367-28381

103. Iimori, M., Watanabe, S., Kiyonari, S., Matsuoka, K., Sakasai, R., Saeki, H., Oki, E., Kitao, H., and Maehara, Y. (2016) Phosphorylation of EB2 by Aurora B and CDK1 ensures mitotic progression and genome stability. *Nat Commun* 7, 11117

104. Luo, Y., Ran, J., Xie, S., Yang, Y., Chen, J., Li, S., Shui, W., Li, D., Liu, M., and Zhou, J. (2016) ASK1 controls spindle orientation and positioning by phosphorylating EB1 and stabilizing astral microtubules. *Cell Discov* 2, 16033

105. Ran, J., Luo, Y., Zhang, Y., Yang, Y., Chen, M., Liu, M., Li, D., and Zhou, J. (2017) Phosphorylation of EB1 regulates the recruitment of CLIP-170 and p150glued to the plus ends of astral microtubules. *Oncotarget* 8, 9858-9867

106. Zhang, Y., Luo, Y., Lyu, R., Chen, J., Liu, R., Li, D., Liu, M., and Zhou, J. (2016) Proto-Oncogenic Src Phosphorylates EB1 to Regulate the Microtubule-Focal Adhesion Crosstalk and Stimulate Cell Migration. *Theranostics* 6, 2129-2140

107. Stenner, F., Liewen, H., Gottig, S., Henschler, R., Markuly, N., Kleber, S., Faust, M., Mischo, A., Bauer, S., Zweifel, M., Knuth, A., Renner, C., and Wadle, A. (2013) RP1 is a phosphorylation target of CK2 and is involved in cell adhesion. *PLoS One* 8, e67595

108. Komarova, Y. A., Huang, F., Geyer, M., Daneshjou, N., Garcia, A., Idalino, L., Kreutz, B., Mehta, D., and Malik, A. B. (2012) VE-cadherin signaling induces EB3 phosphorylation to suppress microtubule growth and assemble adherens junctions. *Mol Cell* 48, 914-925

109. Chen, J., Luo, Y., Li, L., Ran, J., Wang, X., Gao, S., Liu, M., Li, D., Shui, W., and Zhou, J. (2014) Phosphoregulation of the dimerization and functions of end-binding protein 1. *Protein Cell* 5, 795-799

110. Le Grand, M., Rovini, A., Bourgarel-Rey, V., Honore, S., Bastonero, S., Braguer, D., and Carre, M. (2014) ROS-mediated EB1 phosphorylation through Akt/GSK3beta pathway: implication in cancer cell response to microtubule-targeting agents. *Oncotarget* 5, 3408-3423

111. Nakamura, S., Grigoriev, I., Nogi, T., Hamaji, T., Cassimeris, L., and Mimori-Kiyosue, Y. (2012) Dissecting the nanoscale distributions and functions of microtubule-end-binding proteins EB1 and ch-TOG in interphase HeLa cells. *PLoS One* 7, e51442

112. Maurer, S. P., Cade, N. I., Bohner, G., Gustafsson, N., Boutant, E., and Surrey, T. (2014) EB1 accelerates two conformational transitions important for microtubule maturation and dynamics. *Curr Biol* 24, 372-384

113. Fox, J. C., Howard, A. E., Currie, J. D., Rogers, S. L., and Slep, K. C. (2014) The XMAP215 family drives microtubule polymerization using a structurally diverse TOG array. *Mol Biol Cell* 25, 2375-2392

114. Widlund, P. O., Stear, J. H., Pozniakovsky, A., Zanic, M., Reber, S., Brouhard, G. J., Hyman, A. A., and Howard, J. (2011) XMAP215 polymerase activity is built by combining multiple tubulin-binding TOG domains and a basic lattice-binding region. *Proc Natl Acad Sci U S A* 108, 2741-2746

115. Thakur, H. C., Singh, M., Nagel-Steger, L., Kremer, J., Prumbaum, D., Fansa, E. K., Ezzahoini, H., Nouri, K., Gremer, L., Abts, A., Schmitt, L., Raunser, S., Ahmadian, M. R., and Piekorz, R. P. (2014) The centrosomal adaptor TACC3 and the microtubule polymerase chTOG interact via defined C-terminal subdomains in an Aurora-A kinase-independent manner. *J Biol Chem* 289, 74-88

116. Hood, F. E., Williams, S. J., Burgess, S. G., Richards, M. W., Roth, D., Straube, A., Pfuhl, M., Bayliss, R., and Royle, S. J. (2013) Coordination of adjacent domains mediates TACC3-ch-TOG-clathrin assembly and mitotic spindle binding. *J Cell Biol* 202, 463-478

ACKNOWLEDGEMENTS

The authors would like to acknowledge Marv Ruona and Paul Fini for their artistic renderings included in this article. We would also like to thank Mark Borgstrom for his expertise in RStudio.

Imaris at the University of Arizona is supported by a TRIF Space Exploration and Optical Sciences (TRIF-SEOS) grant.

[$$] Data Availability. The mass spectrometry data have been deposited to the ProteomeXchange Consortium via the PRIDE (31) partner repository with the dataset identifier PXD011431 and 10.6019/PXD011431.

Disclaimer: The content is solely the responsibility of the authors and does not necessarily represent the official views of the National Institutes of Health.

Figure Legends

Figure 1. G2L1, MARK2, CLIP2, EB1, AGAP3, and CKAP5 undergo insulin-regulated phosphorylation. ***A***, Serum-starved 3T3-L1 adipocytes were either left untreated or treated with insulin, lysed, and target proteins were immunoprecipitated as described in Experimental Procedures. The IPs were separated by SDS-PAGE and the gel slice corresponding to the protein of interest was excised and subjected to trypsin digestion. The resulting tryptic digest was purified and subsequently analyzed by tandem mass spectrometry. Raw data processing for quantification was executed in Progeneis QI for Proteomics and peptide/protein identification was performed by database searching with Mascot. The resulting Mascot peptide and protein identifications were imported into Progenesis QI for Proteomics and quantification of changes in phosphopeptide abundance was performed via extracted ion abundance in Progenesis QI for Proteomics. MS/MS, tandem mass spectrometry. ***B***, G2L1, MARK2, CLIP2, EB1, AGAP3, and CKAP5 phosphorylation was analyzed as described above and in Experimental Procedures (n=4 per protein). Phosphopeptides are labeled with both the starting and final amino acid position of the phosphopeptide within the protein, along with the phospho-site (in red). The basal versus insulin data is separated by the vertical dashed black line. The horizontal red dashed line represents a 50% decrease in phosphorylation while the horizontal green dashed line represents a 2-fold increase in phosphorylation. *p≤0.05; **p≤0.01 insulin compared to basal; T-test. BAS, basal. INS, insulin. ***C***, The illustration depicts all identified phosphorylation sites affected by insulin, the location of the phosphorylation sites within each protein, the effect of insulin on phosphorylation (increased = green, suppressed = red), as well as the hypothetical localization of the microtubule-regulating proteins respective to the microtubule. TOG, tumor overexpressed gene; UBA, ubiquitin-associated; GAR, Gas2-related; GAP, GTPase-activating protein; KA1, kinase associated domain 1; ANK, ankyrin; EEY/F, EEY/F motif; GLD, GTP-binding protein-like domain; EBH, EB homology; PH, pleckstrin homology.

Figure 2. The G2L1 interactomes. ***A***, To identify new interacting partners for G2L1 in 3T3-L1 adipocytes, different G2L1 IPs were compared against negative control IPs either in the absence or presence of insulin treatment. The IPs were separated by SDS-PAGE, fractionated into gel slices, subjected to trypsin digestion, and analyzed by tandem mass spectrometry. Peptide and protein identification was performed by Mascot database searching, and the resulting spectral count data was assembled with Scaffold. The spectrum count data was then scored for enrichment using SAINT and the resulting SAINT-qualified protein spectral count data was visualized with a Spectrum Count Profile "SCP". The SAINT-qualified proteins from the three alternative G2L1 interactomes performed were then integrated and visualized with Cytoscape. ***B***, 150mm plates of differentiated 3T3-L1 adipocytes either left untreated or infected with mCherry-G2L1-myc overexpressing adenovirus and were lysed in an isotonic CHAPS lysis buffer. IPs were performed as described in Experimental Procedures. The IPs or whole cell lysates were resolved by 10% SDS-PAGE and transferred to nitrocellulose membranes. The membranes containing the immunoprecipitated proteins were subjected to western blot with the antibodies indicated. The labels on the right side of the blot indicate where the various proteins migrate on the gel. MK, protein ladder marker; WB, western blot; WCL, whole cell lysates; MS/MS tandem mass spectrometry. ***C,*** For the various G2L1 interactomes (from top to bottom, endogenous G2L1, mCherry-G2L1-myc, and mCherry-G2L1-myc), the "SAINT-qualified" proteins were ordered in a hierarchical manner, from lowest spectrum counts identified to highest, and results from two experiments were individually plotted in a SCP. Basal NIgG IPs (green), insulin NIgG IPs (magenta), basal G2L1 IPs (red), and insulin G2L1 IPs (turquoise). ***D,*** Cytoscape-based integrated visual representation of the anti-G2L1, anti-myc mCherry-G2L1-myc, and anti-mCherry mCherry-G2L1-myc SAINT-qualified proteins. The proteins listed in turquoise were identified in all three G2L1 interactomes, while the proteins listed in green were shared between the anti-mCherry and anti-myc antibody mCherry-G2L1-myc interactomes.

Figure 3. CLASP2 and G2L1 colocalize in 3T3-L1 adipocytes. ***A-B***, Live-cell imaging of adipocytes cultured in complete media co-expressing mRuby2-Tubulin (magenta) and GFP-CLASP2-HA (***A***, green) or mCherry-G2L1-myc (***B***, green). Live cells were imaged using TIRFM on a 2-second acquisition interval. Time series images to the right of the whole cell image are used to highlight +TIP dynamics within the indicated ROI. ***C***, Immunofluorescence images of adipocytes cultured in complete media co-overexpressing GFP-CLASP2-HA (green) and mCherry-G2L1-myc (magenta). Cells were fixed and immunolabeled for tubulin (inverted white). Bottom row is magnified ROI. ROI, region of interest. Scale bar = 20μm.

Figure 4. The effect of insulin on CLASP2 +TIP dynamics. Live-cell imaging of adipocytes serum-starved for one hour and subsequently stimulated with 100nM insulin. Live cells were imaged using TIRFM on a two-second acquisition interval. ***A***, Single frame of live-cell imaging of adipocytes co-expressing GFP-CLASP2 (green) and mRuby2-Tubulin (magenta) at basal state (top row) or ten minutes (bottom row) following insulin stimulation. CLASP2 is displayed in inverted white to highlight +TIP density. ***B***, Quantification of CLASP2-containing +TIP density per unit area (μm^2) in adipocytes at basal state or ten minutes following insulin stimulation. Percent increase in CLASP2-containing +TIP density is indicated to the right. Statistical comparison made by paired parametric t-test, n = 5 cells. ***C***, Temporally color-coded projection of GFP-CLASP2 localization during a 30 second live-cell imaging interval. The length and extent of color overlap of time-projected CLASP2 localization indicates reduced displacement and hence lower velocity of CLASP2-containing +TIPs during the imaging interval in adipocytes after ten minutes of insulin stimulation. ***D***, Quantification of CLASP2-containing +TIP velocity in adipocytes at basal state or ten minutes following insulin stimulation indicates reduced velocity of CLASP2-containing +TIPS after insulin treatment. Statistical comparison made by unpaired parametric t-test, n = 123-125 CLASP2-containing +TIPS from five cells. Scale bars = 5μm. ***E***, Image of entire cells in the basal state (left panel) or eight minutes post insulin treatment (right panel) extracted from Video 2. Time

series images under the whole cell image are used to highlight insulin-stimulated +TIP dynamics within the indicated ROI. ***F***, Time series extracted from Video 2 of the indicated ROIs at either the basal state or at four minutes post insulin treatment to present an example of changing CLASP2 microtubule plus-end dynamics with insulin stimulation. ***G***, Live cell CLASP2-containing +TIP dynamics of the ROI extracted from Video 2 were captured in the basal state followed by stimulation with insulin. Each insulin-stimulated CLASP2-containing +TIP trail length time point was compared against the basal CLASP2-containing +TIP trail length to test for significant differences. T-test; *p≤0.05, **p≤0.01. Red circles represent outlier data points. ROI, region of interest. BAS, basal. INS, insulin. Scale bar = 10μm.

Figure 5. Insulin stimulates G2L1 plus-end trailing. Live-cell imaging of adipocytes overexpressing mCherry-G2L1-myc (magenta). Adipocytes were serum starved for one hour and subsequently stimulated with 100nM insulin. Live cells were imaged using TIRFM on a two-second acquisition interval and the displayed time series were extracted from Video 3. ***A***, Image of entire cell in the basal state (left panel) or twelve minutes post insulin treatment (right panel). Time series images under the whole cell image are used to highlight insulin-stimulated G2L1-containing +TIP dynamics within the indicated ROI. ***B***, Time series of the indicated ROIs at either the basal state or at four minutes post insulin treatment to present an example of changing G2L1 plus-end dynamics with insulin stimulation. ***C***, Live cell G2L1-containing +TIP dynamics of the ROI were captured in the basal state followed by stimulation with insulin. Each insulin-stimulated G2L1-containing +TIP trail length time point was compared against the basal G2L1-containing +TIP trail length to test for significant differences. T-test; *p≤0.05, **p≤0.01. Red circles represent outlier data points. ROI, region of interest. BAS, basal. INS, insulin. Scale bar = 10μm.

Figure 6. Insulin stimulates CLASP2 and G2L1 microtubule plus-end co-trailing. Live-cell imaging of adipocytes co-overexpressing GFP-CLASP2-HA (green) and mCherry-G2L1-myc (magenta). Adipocytes were serum starved for one hour and subsequently stimulated with 100nM

insulin. Live cells were imaged using TIRFM on a two-second acquisition interval and the displayed time series were extracted from Video 4. ***A***, Image of entire cell in the basal state (left panel) or eight minutes post insulin treatment (right panel). Time series images under the whole cell image are used to highlight insulin-stimulated +TIP dynamics within the indicated ROI. ***B***, Time series of the indicated ROIs at either the basal state or at three minutes post insulin treatment to present an example of changing CLASP2 and G2L1 plus-end dynamics with insulin stimulation. ***C***, Live cell +TIP dynamics of the ROI were captured in the basal state followed by stimulation with insulin. Each insulin-stimulated +TIP trail length time point was compared against the basal +TIP trail length to test for significant differences. T-test; *p≤0.05, **p≤0.01. Red circles represent outlier data points. ROI, region of interest. BAS, basal. INS, insulin. Scale bar = 10μm. ***D***, A model depicting the insulin-stimulated shift of CLASP2 and G2L1 from growing plus-end microtubule localization to “trailing”, a behavior characterized by CLASP2 and G2L1 decorating the trailing microtubule lattice behind the growing microtubule plus-end.

Figure 7. Insulin stimulates acetylation of α-tubulin at Lysine 40 and microtubule stabilization. ***A***, Serum-starved 3T3-L1 adipocytes were either left untreated or treated with an insulin time course for the times indicated. Adipocyte lysis was performed as described in Experimental Procedures. The whole cell lysates were resolved by 10% SDS-PAGE and transferred to nitrocellulose membranes. The membranes were subjected to western blot with the antibodies indicated. Representative blot, n=3. MK, protein ladder marker. AcK40, α-tubulin acetylation at lysine 40. ***B***, Immunofluorescence images of the effect of insulin (30min, 100nM) on serum-starved adipocytes. Cells were fixed and immunolabeled for α-tubulin (white) and AcK40 (inverted white). Scale bar = 10μm. ***C***, Quantification of AcK40 in adipocytes at basal state or ten minutes following insulin stimulation indicates increased AcK40 after insulin treatment. The images were quantified for corrected total cell fluorescence (CTCF) as described in Experimental Procedures. Quantification was based on data collected from 25-40 cells per condition. The

images are representative of five independent experiments. Error bars represent ±SEM and statistical comparison was made by unpaired parametric t-test. ***D***, Immunofluorescence images of the effect of insulin (30min) on nocodazole-induced microtubule depolymerization in serum-starved adipocytes. Cells were left untreated or treated with either 2μM nocodazole alone for 15min or 100nM insulin for 30 min followed by 2μM nocodazole for 15min, fixed and immunolabeled for α-tubulin (inverted white). CTRL, control, NOCO, nocodazole. INS, insulin. Scale bar = 10μm. ***E***, Quantification of microtubule density in adipocytes indicates insulin treatment results in resistance to nocodazole-induced microtubule depolymerization. Quantification was based on data collected from 8-11 cells per condition. The images are representative of two independent experiments. Error bars represent ±SEM and statistical comparison was made by unpaired parametric t-test. ***F***, Serum-starved 3T3-L1 adipocytes were either left untreated or treated with either insulin alone or insulin together with rapamycin pretreatment to inhibit mTOR. Evaluation of AcK40 was performed as described above in *A*. ***G***, Serum-starved 3T3-L1 adipocytes were either left untreated, treated with SB216763 alone (a GSK3 inhibitor), treated with insulin alone, or treated with insulin together with SB216763 pretreatment. Evaluation of AcK40 was performed as described above in *A*. ***H***, Six experiments as performed in *G* were quantified by densitometry to evaluate the effects of SB216763-mediated inhibition of GSK3 on AcK40. The AcK40 signal was normalized to the total α-tubulin signal on the western blots. These values were then normalized by the mean value of the basal sample and then expressed as a fold change over basal ±SEM; T-test. SB, SB216763. ***I,*** In this proposed hypothetical model, GSK3 suppresses the acetylation of α-tubulin at lysine 40 ("AcK40") in the basal state. Insulin deactivates GSK3 and stimulates AcK40 through rapamycin-sensitive mTOR.

FIGURES

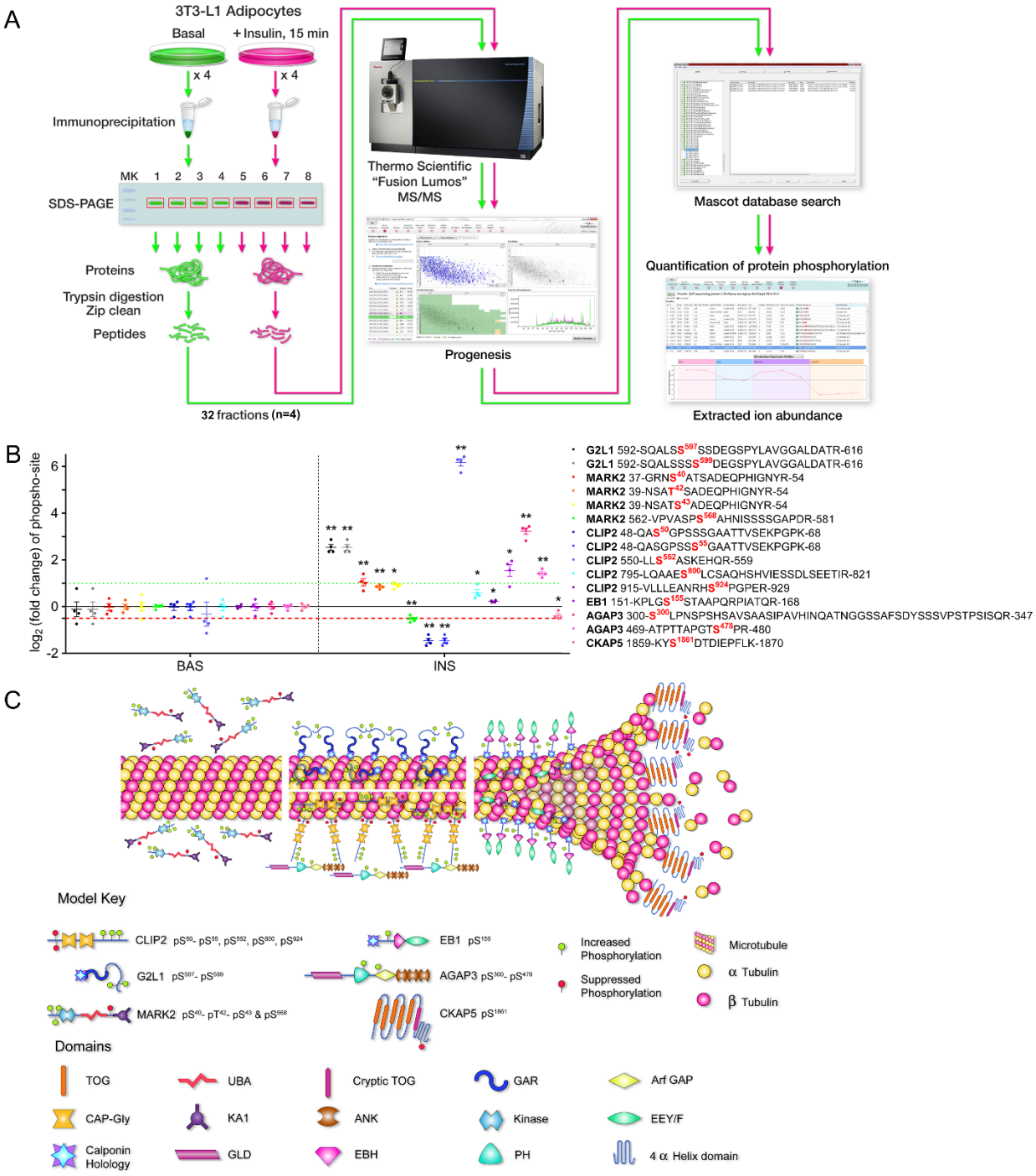

Figure 1

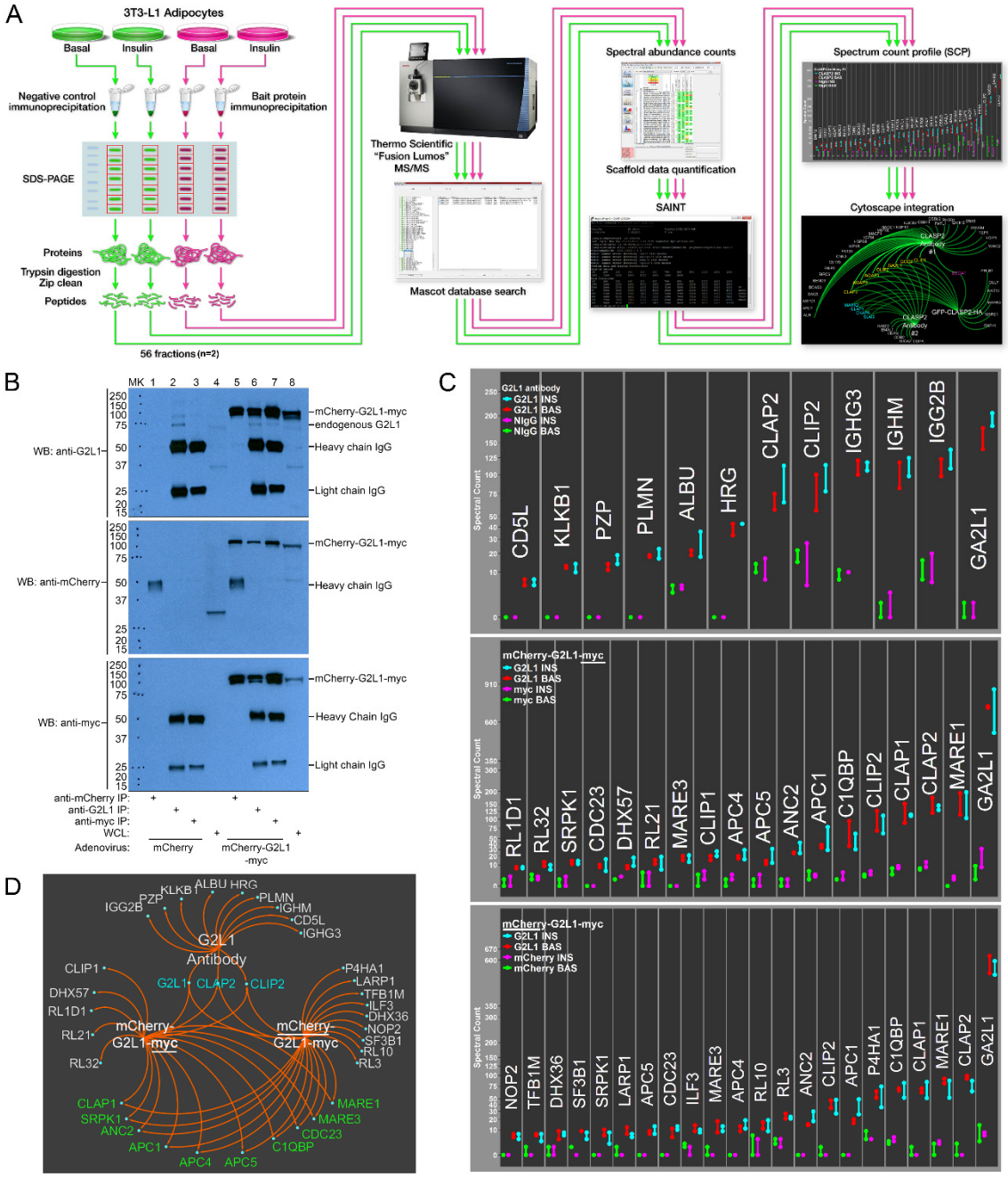
A
3T3-L1 Adipocytes
Basal
Insulin
Basal
Insulin
Negative control immunoprecipitation
Bait protein immunoprecipitation
SDS-PAGE
Proteins
Trypsin digestion Zip clean
Peptides
56 fractions (n=2)
Thermo Scientific "Fusion Lumos" MS/MS
Mascot database search
Spectral abundance counts
Scaffold data quantification
SAINT
Spectrum count profile (SCP)
Cytoscape integration
B
MK 1 2 3 4 5 6 7 8
WB: anti-G2L1
mCherry-G2L1-myc
endogenous G2L1
Heavy chain IgG
Light chain IgG
WB: anti-mCherry
mCherry-G2L1-myc
Heavy chain IgG
WB: anti-myc
mCherry-G2L1-myc
Heavy Chain IgG
Light chain IgG
anti-mCherry IP:
anti-G2L1 IP:
anti-myc IP:
WCL:
Adenovirus:
mCherry
mCherry-G2L1 -myc
C
G2L1 antibody
G2L1 INS
G2L1 BAS
NIgG INS
NIgG BAS
CD5L
KLKB1
PZP
PLMN
ALBU
HRG
CLAP2
CLIP2
IGHG3
IGHM
IGG2B
GA2L1
mCherry-G2L1-myc
G2L1 INS
G2L1 BAS
myc INS
myc BAS
RL1D1
RL32
SRPK1
CDC23
DHX57
RL21
MARE3
CLIP1
APC4
APC5
ANC2
APC1
C1QBP
CLIP2
CLAP1
CLAP2
MARE1
GA2L1
mCherry-G2L1-myc
G2L1 INS
G2L1 BAS
mCherry INS
mCherry BAS
NOP2
TFB1M
DHX36
SF3B1
SRPK1
LARP1
APC5
CDC23
ILF3
MARE3
APC4
RL10
RL3
ANC2
CLIP2
APC1
P4HA1
C1QBP
CLAP1
MARE1
CLAP2
GA2L1
Spectral Count
D
G2L1 Antibody
mCherry-G2L1-myc
mCherry-G2L1-myc
IGG2B
PZP
KLKB1
ALBU HRG
PLMN
IGHM
CD5L
IGHG3
CLIP1
DHX57
RL1D1
RL21
RL32
G2L1
CLAP2
CLIP2
P4HA1
LARP1
TFB1M
ILF3
DHX36
NOP2
SF3B1
RL10
RL3
CLAP1
SRPK1
ANC2
APC1
APC4
APC5
MARE1
MARE3
CDC23
C1QBP

Figure 2

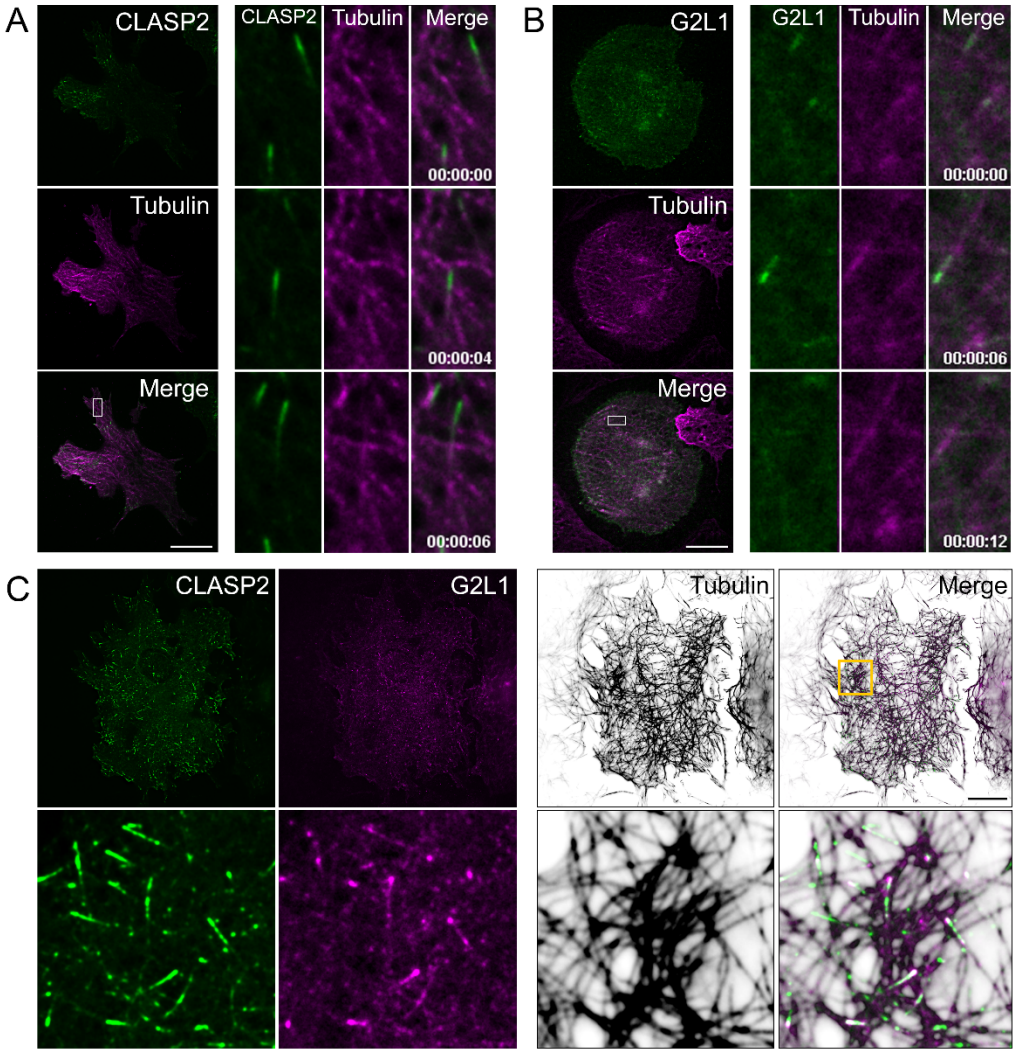
A
CLASP2
CLASP2
Tubulin
Merge
00:00:00
Tubulin
00:00:04
Merge
00:00:06
B
G2L1
G2L1
Tubulin
Merge
00:00:00
Tubulin
00:00:06
Merge
00:00:12
C
CLASP2
G2L1
Tubulin
Merge

Figure 3

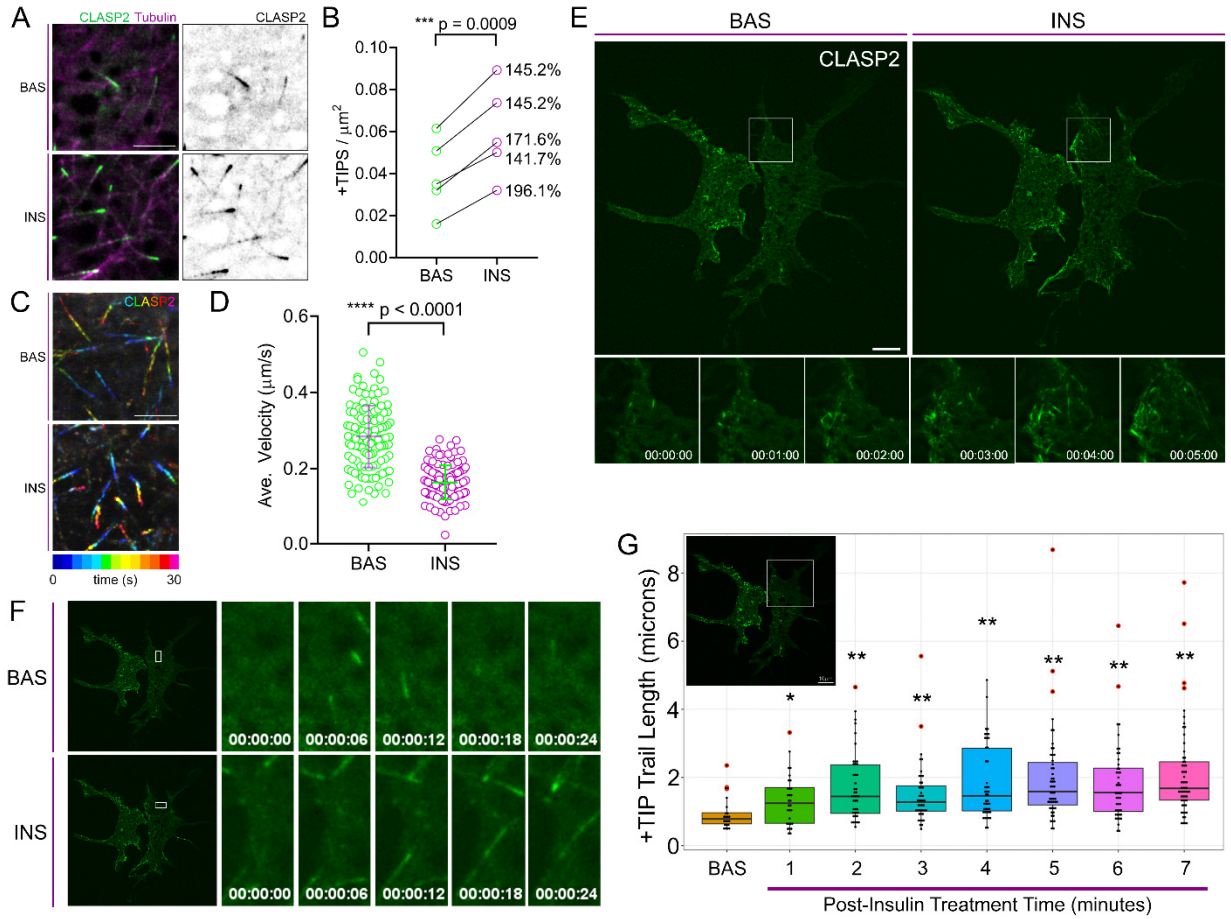
A
CLASP2 Tubulin
CLASP2
BAS
INS
B
*** p = 0.0009
+TIPS / µm²
0.10
0.08
0.06
0.04
0.02
0.00
145.2%
145.2%
171.6%
141.7%
196.1%
BAS
INS
C
CLASP2
BAS
INS
0
time (s)
30
D
**** p < 0.0001
Ave. Velocity (µm/s)
0.6
0.4
0.2
0.0
BAS
INS
E
BAS
INS
CLASP2
00:00:00
00:01:00
00:02:00
00:03:00
00:04:00
00:05:00
F
BAS
INS
00:00:00
00:00:06
00:00:12
00:00:18
00:00:24
G
+TIP Trail Length (microns)
8
6
4
2
0
BAS
1
2
3
4
5
6
7
Post-Insulin Treatment Time (minutes)

Figure 4

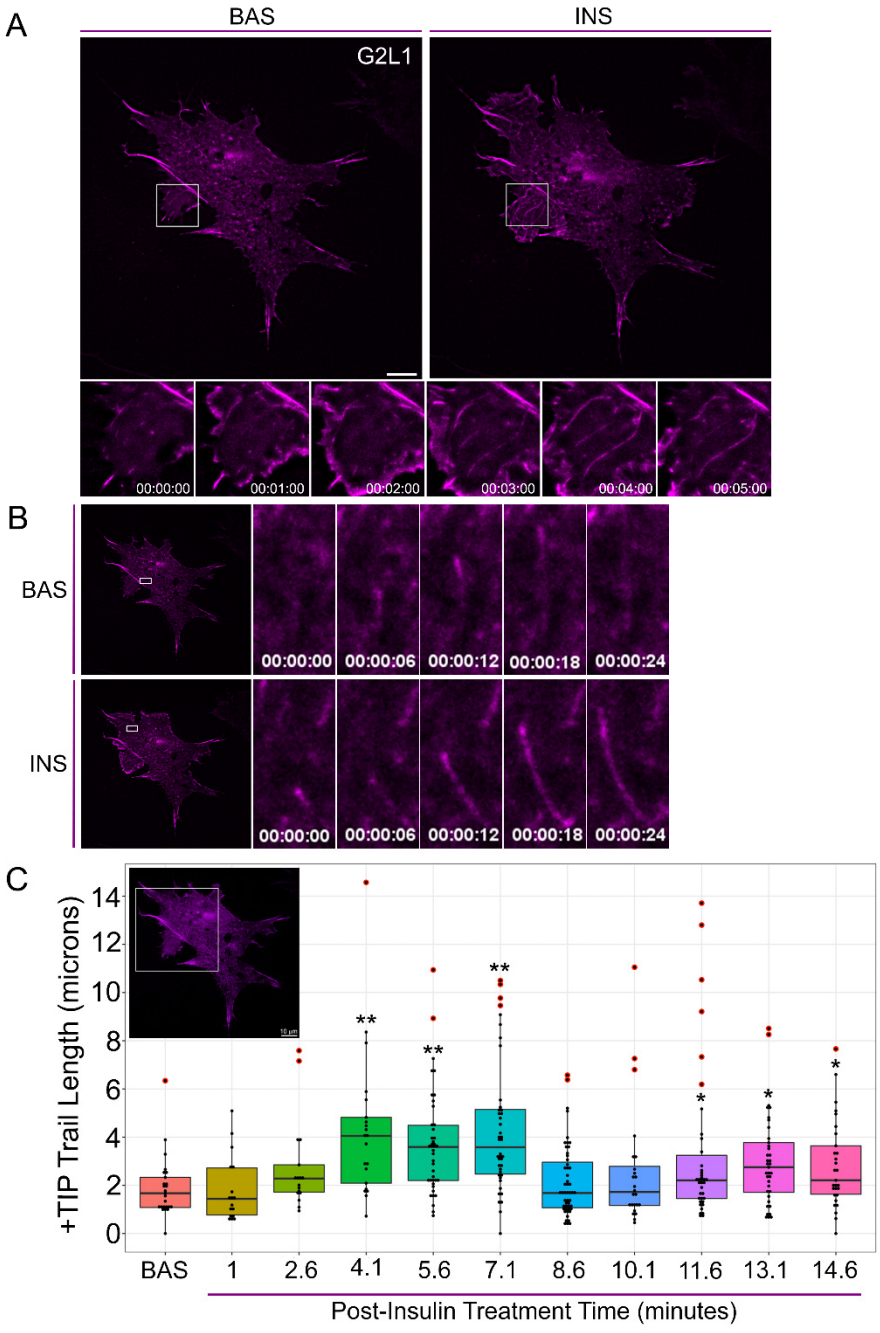
A
BAS
INS
G2L1
00:00:00
00:01:00
00:02:00
00:03:00
00:04:00
00:05:00
B
BAS
INS
00:00:00
00:00:06
00:00:12
00:00:18
00:00:24
C
+TIP Trail Length (microns)
0
2
4
6
8
10
12
14
BAS
1
2.6
4.1
5.6
7.1
8.6
10.1
11.6
13.1
14.6
Post-Insulin Treatment Time (minutes)

Figure 5

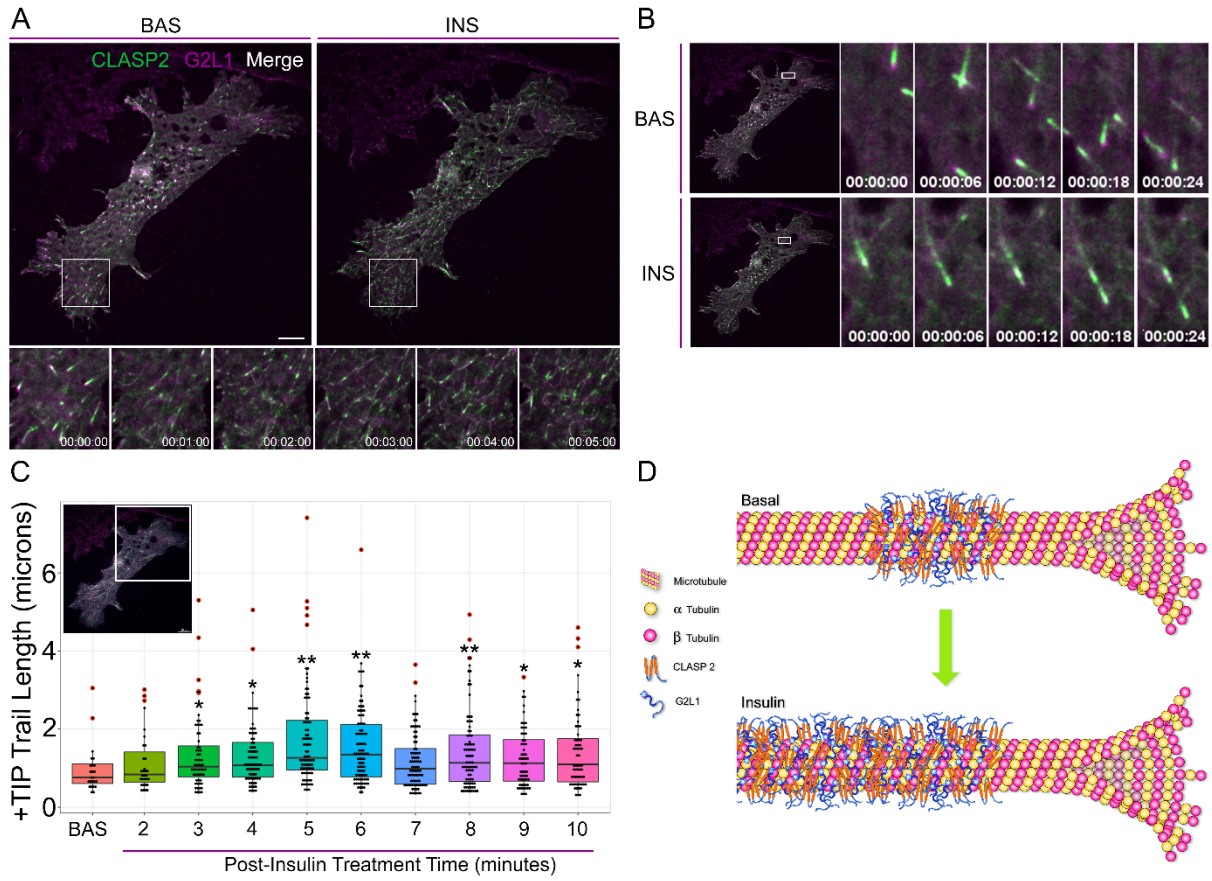
A
BAS
INS
CLASP2 G2L1 Merge
00:00:00
00:01:00
00:02:00
00:03:00
00:04:00
00:05:00
B
BAS
INS
00:00:00
00:00:06
00:00:12
00:00:18
00:00:24
C
+TIP Trail Length (microns)
0
2
4
6
BAS
2
3
4
5
6
7
8
9
10
Post-Insulin Treatment Time (minutes)
D
Basal
Insulin
Microtubule
α Tubulin
β Tubulin
CLASP 2
G2L1

Figure 6

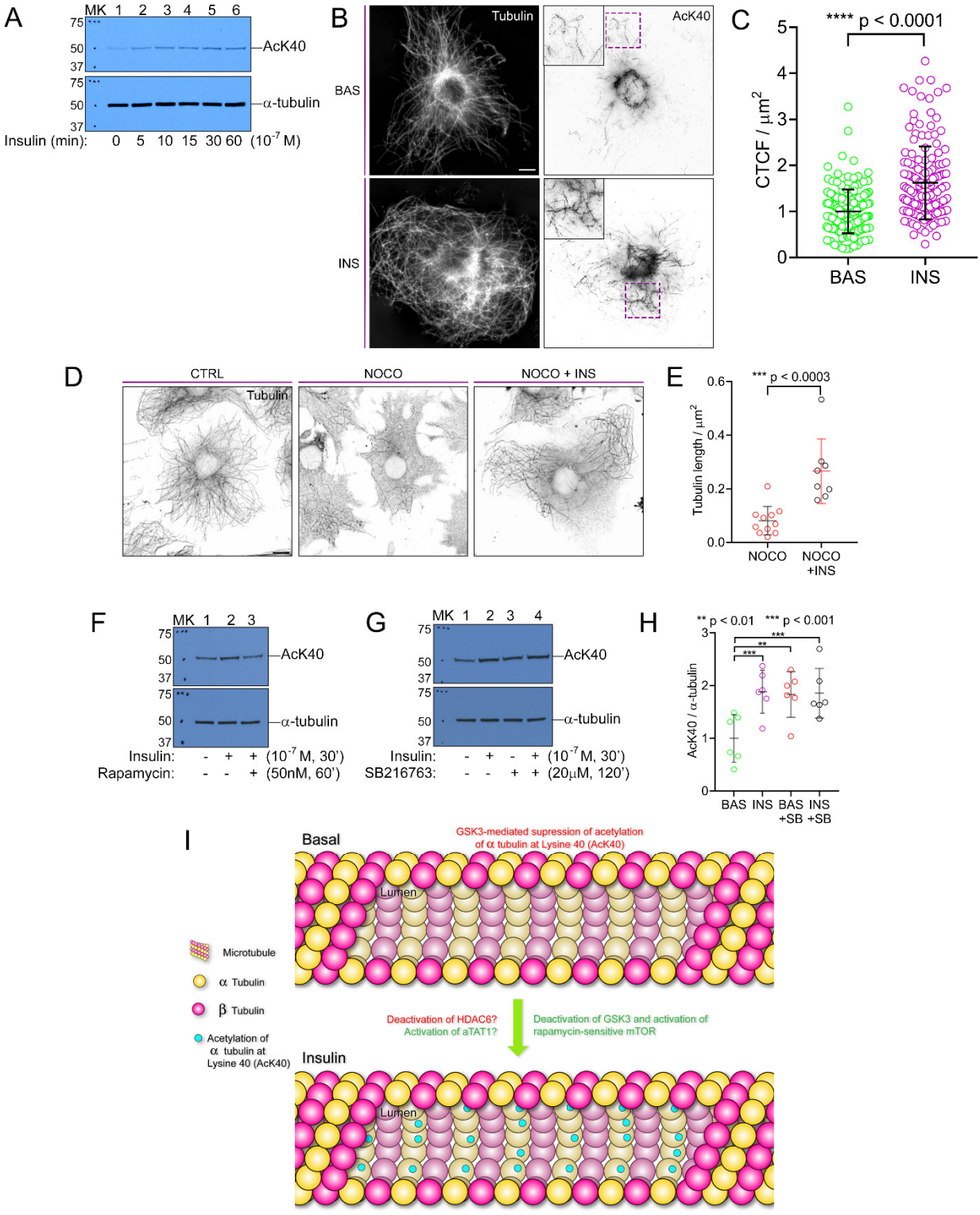
A
MK 1 2 3 4 5 6
75
50
37
AcK40
α-tubulin
Insulin (min): 0 5 10 15 30 60 (10-7 M)
B
Tubulin
AcK40
BAS
INS
C
**** p < 0.0001
CTCF / µm2
BAS
INS
D
CTRL
NOCO
NOCO + INS
Tubulin
E
*** p < 0.0003
Tubulin length / µm2
NOCO
NOCO +INS
F
MK 1 2 3
AcK40
α-tubulin
Insulin: - + + (10-7 M, 30')
Rapamycin: - - + (50nM, 60')
G
MK 1 2 3 4
AcK40
α-tubulin
Insulin: - + - + (10-7 M, 30')
SB216763: - - + + (20µM, 120')
H
** p < 0.01 *** p < 0.001
AcK40 / α-tubulin
BAS INS BAS +SB INS +SB
I
Basal
GSK3-mediated supression of acetylation of α tubulin at Lysine 40 (AcK40)
Lumen
Microtubule
α Tubulin
β Tubulin
Acetylation of α tubulin at Lysine 40 (AcK40)
Deactivation of HDAC6? Activation of aTAT1?
Deactivation of GSK3 and activation of rapamycin-sensitive mTOR
Insulin
Lumen

Figure 7